Chemical Science

EDGE ARTICLE

View Article Online
View Journal | View Issue

Cite this: *Chem. Sci.*, 2015, **6**, 5601

In vivo demonstration of an active tumor pretargeting approach with peptide nucleic acid bioconjugates as complementary system†

Anna Leonidova,‡[a] Christian Foerster,‡§[b] Kristof Zarschler,[b] Maik Schubert,[b] Hans-Jürgen Pietzsch,[b] Jörg Steinbach,[b] Ralf Bergmann,[b] Nils Metzler-Nolte,[c] Holger Stephan*[b] and Gilles Gasser*[a]

Received 16th March 2015
Accepted 16th June 2015

DOI: 10.1039/c5sc00951k

www.rsc.org/chemicalscience

A novel, promising strategy for cancer diagnosis and therapy is the use of a pretargeting approach. For this purpose, the non-natural DNA/RNA analogues Peptide Nucleic Acids (PNAs) are ideal candidates as *in vivo* recognition units due to their high metabolic stability and lack of unspecific accumulation. In the pretargeting approach, an unlabeled, highly specific antibody–PNA conjugate has sufficient time to target a tumor before administration of a small fast-clearing radiolabeled complementary PNA that hybridizes with the antibody–PNA conjugate at the tumor site. Herein, we report the first successful application of this multistep process using a PNA-modified epidermal growth factor receptor (EGFR) specific antibody (cetuximab) and a complementary ^{99m}Tc-labeled PNA. *In vivo* studies on tumor bearing mice demonstrated a rapid and efficient *in vivo* hybridization of the radiolabeled PNA with the antibody–PNA conjugate. Decisively, a high specific tumor accumulation was observed with a tumor-to-muscle ratio of >8, resulting in a clear visualization of the tumor by single photon emission computed tomography (SPECT).

Introduction

The excellent target specificity of monoclonal antibodies (mAbs) renders this class of biomacromolecules a beneficial platform to detect and treat tumor malignancies. In nuclear medicine, such tumor antigen-specific vehicles labeled with radionuclides would be applicable for non-invasive imaging of diseases and more importantly, for *in vivo* delivery of therapeutically relevant radioactivity doses to tumor sites. Unfortunately, the concept of utilizing radionuclide-carrying tumor-specific mAbs is afflicted with several drawbacks,[1–3] mainly arising from the high molecular weight of mAbs (~150 kDa). Due to size-related limitations in passing biological barriers,[4] such as extravasation and the inability of glomerular filtration, mAbs exhibit a slow but gradual accumulation in tumor sites and long blood retention times of up to several days, respectively.[5] The slow blood clearance rate of mAbs forces extensive waiting times before acquiring a diagnostic image with reasonable signal-to-background ratio as well as to label with appropriate isotopes.[6,7] Detrimental radiation exposure for almost all tissues in the organism, especially during therapeutic applications, will be the result of their prolonged blood pool retention time.[8] Despite innumerable research activities and efforts conducted so far, only two drugs, namely Bexxar® and Zevalin™, representing radiolabeled mAbs for treatment of Non-Hodgkin's lymphoma are currently approved by the FDA.[9–11]

An attractive strategy to circumvent these limitations is the use of a pretargeting approach that involves an artificial *in vivo* recognition system composed of a nonradioactive antibody conjugate and a small radiolabeled "effector" molecule. As schematically represented in Scheme 1, in this multistep process, an unlabeled, highly tumor-specific antibody conjugate is first administrated into a patient. Upon injection, sufficient

[a]*Department of Chemistry, University of Zurich, Winterthurerstrasse 190, CH-8057 Zurich, Switzerland. E-mail: gilles.gasser@chem.uzh.ch; Web: http://www.gassergroup.com; Tel: +41 44 635 46 30*

[b]*Helmholtz-Zentrum Dresden – Rossendorf, Institute of Radiopharmaceutical Cancer Research, Bautzner Landstraße 400, D-01328 Dresden, Germany. E-mail: h.stephan@hzdr.de; Web: http://www.hzdr.de/NanoscalicSystems; Tel: +49 351 260-3091*

[c]*Lehrstuhl für Anorganische Chemie I – Bioanorganische Chemie, Fakultät für Chemie und Biochemie, Ruhr-Universität Bochum, Universitätsstrasse 150, D-44801 Bochum, Germany*

† Electronic supplementary information (ESI) available: Characterization of the PNAs used this study (Fig. S1–14), radio HPLC of **[^{99m}Tc](Tc-Dpa)-(Cys-PEG$_{10kDa}$)-PNA** (Fig. S15), melting temperatures (T_M) for three complementary 17-mer PNA systems (Table S1), melting curves of different PNAs (Fig. S16), radio HPLC of the **[^{99m}Tc](Tc-Dpa)-(Cys-PEG$_{10kDa}$)-PNA** (original), in rat arterial blood plasma (Fig. S17), biodistribution of radiolabeled PNAs in Wistar rats (%ID mean ± SD) (Table S2), biodistribution of radiolabeled PNAs in Wistar rats (SUV mean ± SD) (Table S3), SPECT/CT comparison of the biodistribution of **[^{99m}Tc](Tc-Dpa)-(Cys-PEG$_{10kDa}$)-PNA** in rat and mouse (Fig. S18). See DOI: 10.1039/c5sc00951k

‡ These authors have contributed equally to the work.

§ Current address: Department of Oncology, University of Alberta, 11560 University Avenue, Edmonton, Alberta, T6G1Z2, Canada.

time is allowed for the antibody conjugate to reach the tumor and to be eliminated from the non targeted tissues. This is then followed by the administration of a small fast-clearing radiolabeled "effector" molecule that binds to the antibody conjugate at the tumor site.[12,13] This approach allows for the rational use of long-circulating high-affinity mAbs for both non-invasive cancer radioimmunodetection and radioimmunotherapy.[14,15]

Several recognition systems have been investigated and to some extend clinically tested for different pretargeting approaches. Most prominent among them are streptavidin/biotin,[16–19] bispecific antibody/hapten[20–27] and synthetic complementary oligonucleotides/oligonucleotides such as morpholino and peptide nucleic acid derivatives.[28–34] For more detailed information and secondary references, we highly recommend the review article of Goldenberg *et al.*[35] Beside the "classical" recognition by supramolecular motifs, bio-orthogonal and ultra-fast click reactions have also been developed as complementary system *in vivo*.[36–39]

Among the range of synthetic oligonucleotides investigated for pretargeting, phosphorodiamidate morpholino oligomers (MORFs) and Peptide Nucleic Acids (PNAs, Scheme 1) have emerged as promising candidates. Both derivatives are non-charged mimics of the naturally occurring ribonucleic acids DNA and RNA. They exhibit a suitable degree of water solubility, are almost inert towards degradation *in vivo*,[40,41] and insensitive towards chemical modifications even under harsh conditions. The superior intrinsic properties of PNAs over DNA/RNA have made them extremely interesting candidates for applications in (nuclear) medicine or biology. Radiolabeled PNA oligomers were indeed utilized as probes for molecular imaging of target specific mRNA sequences.[42–48] However, the relatively low cellular uptake of PNAs has represented a serious drawback, which has undoubtedly delayed their use as antisense or antigen agents, although several techniques are now available to overcome this problem (*e.g.* use of cell-penetrating peptides, *etc.*). Nonetheless, the limited cellular uptake of PNAs creates a very interesting bio-orthogonal system. Indeed, administration of a radiolabeled PNA strand into a living organism rarely results into unspecific binding.[34,48] In other words, the PNA strand is usually excreted in its intact form from the kidney/liver. This characteristic, in addition to the excellent physicochemical properties discussed above, have made PNAs a promising tool in the tumor pretargeting approach.

Pioneering work in this field of research was performed by Hnatowich and co-workers, who demonstrated a first proof-of-concept in 1997.[32–34,49] In those studies, surrogates such as PNA-loaded polymeric[32,34] and agarose-based avidin beads[49] transplanted into mouse thighs were used. To the best of our knowledge, there is only a single report describing the utilization of PNA–streptavidin bioconjugates for (non-specific) tumor localization in a mouse model by passive diffusion.[33] These PNA–protein conjugates were found to accumulate unspecifically in most tissues of the animals. Consequently, upon administration of the radiolabeled complementary PNA, radioactivity levels were significantly higher compared to control animals. However, tumor antigens have not been specifically targeted by anti-tumor antibody–PNA conjugates yet. Thus, a critical evaluation of a tumor pretargeting concept *in vivo* is still lacking.

In this work, we aim to demonstrate the suitability of PNA-based bioconjugates as versatile complementary system for the specific transportation and accumulation of radionuclides in tumors. More specifically, in this article, we first describe the preparation and characterization of several PNA bioconjugates that contained different building blocks such as a 2,2′-dipicolylamine (Dpa) to chelate the radioactive ^{99m}Tc as well as polyethylene glycol (PEG) units to tune the biodistribution of the PNA oligomers. In addition, radiolabeling of the Dpa-containing bioconjugates with $[^{99m}Tc]Tc(H_2O)_3(CO)_3^+$ as well as detailed radiopharmaceutical evaluation including biodistribution and metabolic profiling is presented.

Of note, to critically assess the PNA-based pretargeting system used in this work, the well-studied, FDA-approved therapeutic mAb cetuximab (C225; Erbitux®, ImClone LLC) was selected, since it is commercially available and shows chemical robustness as well as a high affinity to a clinically relevant tumor biomarker.[50–54] The molecular target of cetuximab, namely the epidermal growth factor receptor (EGFR),[55,56] is involved in regulating cell growth, differentiation and survival of cells.[57,58] In a variety of human malignancies, EGFR is constitutively activated as a result of receptor overexpression, mutation or deregulation[59–61] and has therefore been investigated as a major target for the treatment of uncontrolled tumor growth.[62–64] All in all, this article demonstrates, for the first time, the successful tumor pretargeting approach using radiolabeled PNAs in combination with PNA–antibody bioconjugates in murine xenografts (human squamous carcinoma cell line A431). This report highlights the immense potential of this approach for both cancer radioimmunodetection as well as radioimmunotherapy.

Results and discussion

Synthesis and characterization of PNA bioconjugates

All PNA oligomers and bioconjugates were synthesized manually on TentaGel S Fmoc-Lys(Boc)-RAM resin using commercially available Fmoc/Bhoc-protected PNA monomers and standard protocols previously reported by our groups.[65] For sufficient stability of PNA–PNA hybrids, complementary PNA oligomers consisting of 17 bases were designed. Table 1 summarizes the PNA sequences used in this work. In order to radiolabel PNA with $[^{99m}Tc]Tc(H_2O)_3(CO)_3^+$, 2,2′-dipicolylamine (Dpa) was site-specifically introduced by copper-mediated 1,3-dipolar cycloaddition ("Click" Chemistry) as previously reported by our groups.[66] In order to improve the pharmacokinetics and bioavailability of compounds and drug carriers, we envisaged PEGylating the PNA bioconjugates as described in the literature for different biomolecules.[67–73] However, in the different studies having investigated the use of PEG-containing PNAs oligomers, the full impact of PEGylation on PNA's pharmacokinetics and biodistribution was not assessed.[65,74–82]

Of note, some of us recently demonstrated that PEGylation of 17-mer L-configured DNA-oligonucleotides – another promising complementary system – significantly altered

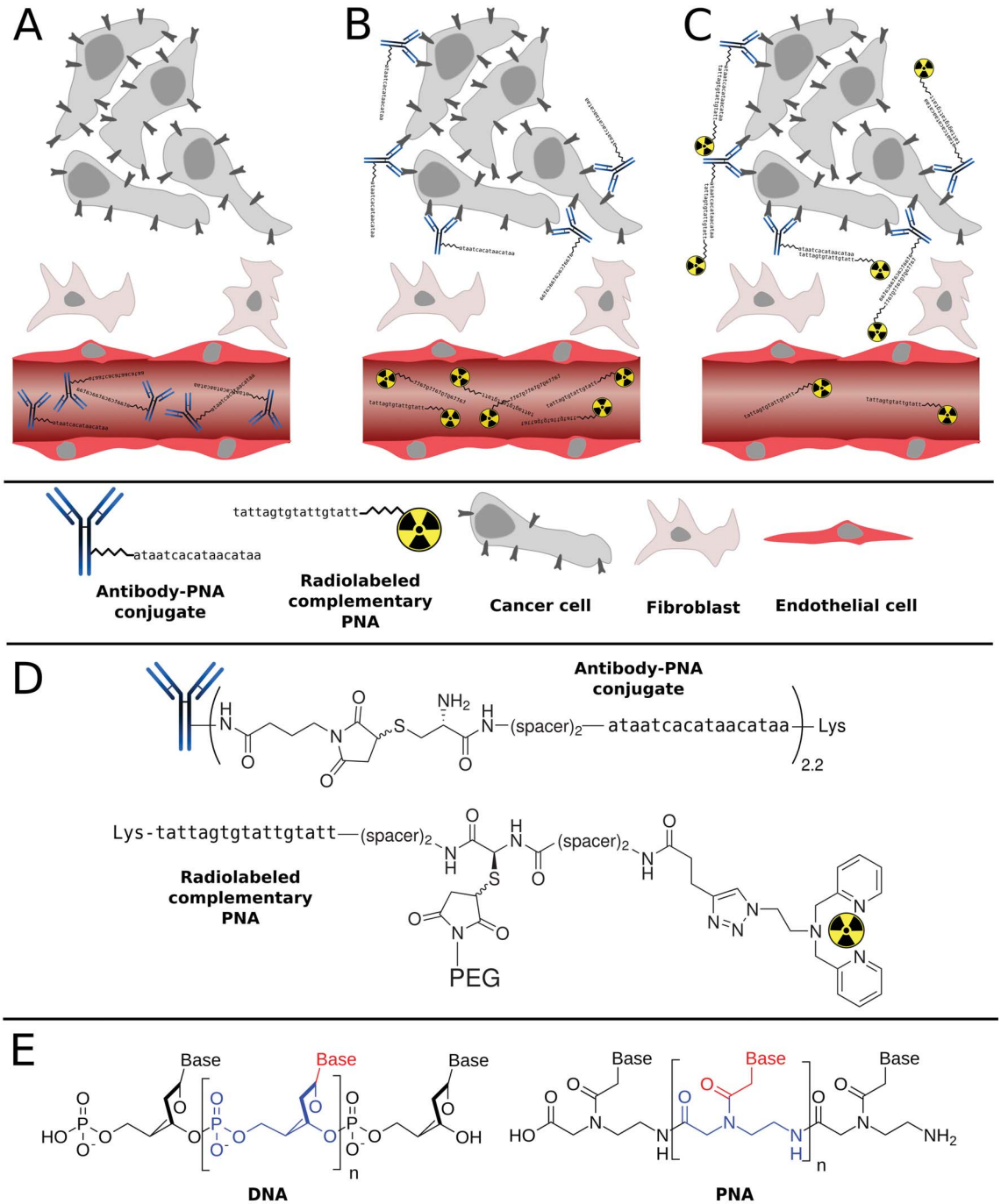

Scheme 1 General principle of tumor pretargeting using Peptide Nucleic Acids (PNA). Firstly, unlabeled, highly specific antibody–PNA conjugates are administered intravenously into the patient (A). After accumulation of the antibody conjugates at the tumor site and clearance from non-target tissues, small fast-clearing radiolabeled complementary PNAs are injected (B), that hybridize with antibody–PNA conjugates (C). The radioactivity symbols inserted into the 2,2′-dipicolylamine (Dpa) chelator illustrate either $^{99m}Tc(CO)_3$ or $^{186}Re(CO)_3$, which are used for diagnosis or therapy, respectively (D). While DNA has a deoxyribose sugar backbone, the PNA's backbone is composed of repeating *N*-(2-aminoethyl)-glycine units linked by amide bonds. Their various purine and pyrimidine bases are linked to the backbone by a methylene bridge and a carbonyl group (E).

radiopharmacokinetics. Indeed, a non-specific accumulations in kidneys was markedly reduced by 90%, while the blood circulation half-life was strongly increased by factor of 4.[83] More specifically, in this work, two different PNA bioconjugates, namely **Dpa-PNA** and **Dpa-Cys-PNA** (Entries 1 and 2 in Table 1), were first synthesized as radionuclide carriers. Maleimido-PEG derivatives (2 and 10 kDa) were then inserted *via* Michael-type addition into the cysteine-containing PNA **Dpa-Cys-PNA** to give **Dpa-(Cys-PEG$_{2kDa}$)-PNA** and **Dpa-(Cys-PEG$_{10kDa}$)-PNA**, respectively (Entries 4 and 5 in Table 1). For this purpose, pretreatment

Table 1 Summary of the PNA oligomers used in this study

Entry	Abbreviation	Sequence[a]
1	**Dpa-PNA**	H-Dpa-spacer-spacer-ttatgttatgtgattat-Lys-NH_2
2	**Dpa-Cys-PNA**	H-Dpa-spacer-spacer-Cys-spacer-spacer-ttatgttatgtgattat-Lys-NH_2
3	**Cys-c-PNA**	H-Cys-spacer-spacer-ataatcacataacataa-Lys-NH_2
4	**Dpa-(Cys-PEG$_{2kDa}$)-PNA**	H-Dpa-spacer-spacer-(Cys-PEG_{2kDa})-spacer-spacer-ttatgttatgtgattat-Lys-NH_2
5	**Dpa-(Cys-PEG$_{10kDa}$)-PNA**	H-Dpa-spacer-spacer-(Cys-PEG_{10kDa})-spacer-spacer-ttatgttatgtgattat-Lys-NH_2
6	**(NOTA)$_3$-C225-Cys-c-PNA**	$(NOTA)_3$-C225-mal-Cys-spacer-spacer-ataatcacataacataa-Lys-NH_2

[a] Spacer = $-NH(CH_2)_2O(CH_2)_2OCH_2CO-$.

of **Dpa-Cys-PNA** with the strong reducing agent tris(2-carboxyethyl)phosphine (TCEP) was found to be necessary to improve the yields of conjugation reaction by preventing PNA–PNA disulfide dimer formation.[74,80] Prior to the addition of maleimido-PEG derivatives, excessive TCEP was removed by size exclusion chromatography to avoid reduction of C–C double bond of maleimide entity leading to sulfhydryl-unreactive succinimide derivatives. In addition, a cysteine-containing PNA oligomer, **Cys-c-PNA** (Entry 3 in Table 1), which is complementary to the other PNA sequences of this study, was prepared. The identity of all PNA analogues **Dpa-PNA**, **Dpa-Cys-PNA**, **Cys-c-PNA**, **Dpa-(Cys-PEG$_{2kDa}$)-PNA**, and **Dpa-(Cys-PEG$_{10kDa}$)-PNA** was confirmed by ESI-MS and MALDI-TOF MS. The high purity of the bioconjugates was verified by LC-MS (Fig. S2, S5, S8, S10 and S12†). Apart from the $[M + nH]^{n+}$ peaks, additional $[M + Cu + nH]^{n+}$, $[M - picolyl + Cu + nH]^{n+}$ were also observed in both ESI and MALDI-TOF spectra for Dpa-containing products. This effect is due to the traces of copper ions still present after the introduction of Dpa to PNA sequence by "Click" Chemistry. Due to the polydispersity of PEG polymers combined with the multiple charged conjugates, ESI-MS generated spectra with multitudinous *m*/*z* peaks disabling conclusive results. The presence of **Dpa-(Cys-PEG$_{2kDa}$)-PNA** and **Dpa-(Cys-PEG$_{10kDa}$)-PNA** was, however, unambiguously confirmed by MALDI-TOF, where only single and double positive charged species were observed (Fig. S11, S13†).

Hybridization properties

In order to assess self-complementary interactions between the PNA strands, we performed UV-based melting curves for each single stranded PNA oligomers, namely **Cys-c-PNA**, **Dpa-PNA**, **Dpa-(Cys-PEG$_{2kDa}$)-PNA** and **Dpa-(Cys-PEG$_{10kDa}$)-PNA**. As displayed in Fig. S16†, no homo-hybridization was observed. In the case of hetero-hybridization, our data listed in Table S1† show that, even at room temperature, **Cys-c-PNA** forms perfect hybrids with all other PNA derivatives (complete match). The determined melting temperatures were almost independent of the degree of PEGylation.

Bioconjugation between Cys-c-PNA and cetuximab

Cetuximab (C225; Erbitux®, ImClone LLC), a chimeric human-murine IgG1 monoclonal antibody, binds specifically to the extracellular domain of the epidermal growth factor receptor (EGFR) on both normal and tumor cells, and competitively inhibits the binding of epidermal growth factor (EGF) as well as other ligands. EGFR is often overexpressed in human malignancies and is associated with poor clinical prognosis.[84,85] Cetuximab binding to EGFR blocks phosphorylation. This blockage results in inhibition of downstream cellular processes such as induction of apoptosis and cell growth. Due to its promising antitumor activity, cetuximab has been approved for the treatment of colorectal and head and neck squamous cell carcinoma as well as with external radiotherapy for the treatment of head and neck squamous cell carcinoma.[86] Of note, we have recently shown that cetuximab labeled with the therapeutic β-emitter ^{90}Y could improve permanent local tumor control after external radiotherapy.[52] Since this well-studied anti-EGFR antibody possesses a high affinity to its molecular target, shows chemical robustness and is commercially available, we selected it as model for radiopharmaceutical evaluation of our PNA-based pretargeting system.

Prior to attachment of **Cys-c-PNA** to cetuximab, the anti-EGFR antibody was modified with 1,4,7-triazacyclononane-1,4,7-triacetic acid (NOTA),[87] a suitable $[^{64}Cu]Cu^{2+}$ chelator for PET-monitoring of aspired PNA–cetuximab bioconjugate.[88–91] This allows us to quantify such important parameters as blood circulation half-life and tumor accumulation of PNA–cetuximab and therefore to optimize the administration regime of PNA–cetuximab conjugate and radiolabeled PNA. NOTA was successfully conjugated to cetuximab resulting in an average of three NOTA molecules per antibody to give **(NOTA)$_3$-C225**.

Subsequent introduction of a maleimido group to **(NOTA)$_3$-C225** was successfully performed by reaction of **(NOTA)$_3$-C225** with 4-maleimido-butyric acid *N*-succinimidyl ester (GMBS) to obtain **(NOTA)$_3$-C225-mal**.

Finally, **Cys-c-PNA** was linked to **(NOTA)$_3$-C225-mal** under mild reaction conditions to give the bioconjugate **(NOTA)$_3$-C225–Cys-c-PNA** (Entry 6 in Table 1). The average number of conjugated **Cys-c-PNA** to **(NOTA)$_3$-C225-mal** was quantified by determination of the absorbance ratio 260 nm/280 nm in the UV spectrum.[92–94] Based on this method, 2.2 ± 0.7 **Cys-c-PNA** moieties per antibody were found. MALDI-TOF MS analysis confirmed this result since the determined number of 2.4 bound PNA oligomers per antibody is in the same range as calculated by UV method (see Fig. S14†).

Radiochemistry

^{99m}Tc-radiolabeling of **Dpa-PNA**, **Dpa-(Cys-PEG$_{2kDa}$)-PNA** and **Dpa-(Cys-PEG$_{10kDa}$)-PNA** was performed *via* the precursor

Table 2 Partition coefficients log $D_{o/w}$ of radiolabeled PNA conjugates at different pH values[a]

pH value	12-mer [^{99m}Tc](Tc-Dpa)-PNA from ref. 48	17-mer [^{99m}Tc](Tc-Dpa)-PNA	17-mer [^{99m}Tc](Tc-Dpa)-(Cys-PEG$_{2kDa}$)-PNA	17-mer [^{99m}Tc](Tc-Dpa)-(Cys-PEG$_{10kDa}$)-PNA
7.2	−0.86	−(2.35 ± 0.04)	−(2.28 ± 0.07)	−(2.40 ± 0.02)
7.4	−0.85	−(2.22 ± 0.03)	−(2.20 ± 0.02)	−(2.22 ± 0.04)
7.6	−0.84	−(2.35 ± 0.07)	−(2.42 ± 0.06)	−(2.35 ± 0.02)

[a] Shown are the averages of three independent experiments with the standard deviation in parentheses.

$[^{99m}Tc(H_2O)_3(CO)_3]^+$ generated by the IsoLink® kit "Carbonyl Labeling Agent".[95] Highly concentrated $[^{99m}Tc(H_2O)_3(CO)_3]^+$ precursor with radiochemical yields (rcy) of >95% was obtained by concentrating the solution at 100 °C for 30 min. Up to 580 MBq of ^{99m}Tc precursor was added to 10 nmol of each of the Dpa-bearing PNA conjugates to give the corresponding radiolabeled PNA conjugates with rcy >95% and high effective specific activities of up to 58 GBq μmol^{-1} (n = 19). Detailed studies to improve radiolabeling conditions have shown a strong dependency of rcy on the pH of the radiolabeling mixture. Radiolabeling at pH < 7 resulted in incomplete complexation of $[^{99m}Tc(CO)_3]^+$ with rcy of <85%, while the rcy went to up to >95% at optimized conditions (70 °C, 40 min, 10 nmol of PNA conjugate) when pH in the range from 7 to 8 was applied.

After purification of ^{99m}Tc-labeled PNA derivatives by HPLC, partition experiments were performed in 1-octanol/buffer systems to assess the lipophilicity/hydrophobicity of the radiolabeled PNAs. Distribution ratio log $D_{o/w}$ was determined at three different pH values (Table 2). Surprisingly, the log D values were almost independent on the degree of PEGylation within the tested pH range (7.2–7.6). Compared with previously published results based on a 12-mer PNA conjugate,[48] it appears that the hydrophilicity is increased more by the lengthening of the PNA chain from 12-mer to 17-mer, rather than by the PEGylation.

In order to examine if the modification of cetuximab with **Cys-c-PNA** resulted in loss of affinity to the EGFR, the antibody derivatives **(NOTA)$_3$-C225** and **(NOTA)$_3$-C225-Cys-c-PNA** were radiolabeled with $[^{64}Cu]CuCl_2$. Of note, the pH of the $[^{64}Cu]CuCl_2$ labeling solution had to be adjusted to around 6 prior addition to the solutions containing the cetuximab conjugates to avoid antibody denaturation. In addition, due to the sensitivity of the antibody, mild reaction conditions (30 °C without shaking) were used. **(NOTA)$_3$-C225** and **(NOTA)$_3$-C225-Cys-c-PNA** were labeled with effective specific activities of up to 16.7 GBq μmol^{-1} and radiochemical yields >99%.

Affinity of [^{64}Cu]Cu-(NOTA)$_3$-C225-Cys-c-PNA and [^{64}Cu]Cu-(NOTA)$_3$-C225 to the EGFR

In order to evaluate the influence of PNA-conjugation on the antibody's binding specificity and affinity to human EGFR, the dissociation characteristics of **[^{64}Cu]Cu-(NOTA)$_3$-C225-Cys-c-PNA** and **[^{64}Cu]Cu-(NOTA)$_3$-C225** were determined comparatively using two dimensional cell cultures of epidermoid carcinoma (A431) and squamous carcinoma (FaDu) cells. These tumor cell lines present different expression levels of the receptor on their cell surface.[96]

Fig. 1 shows the saturation binding curves of radiolabeled cetuximab conjugates for both cell lines. For **[^{64}Cu]Cu-(NOTA)$_3$-C225-Cys-c-PNA** and **[^{64}Cu]Cu-(NOTA)$_3$-C225**, Scatchard analysis was applied to determine dissociation constants (Table 3). A K_d of 5.4 ± 0.9 nM and B_{max} of 13.3 pmol per mg protein for A431 and a K_d of 1.1 ± 0.2 nM and B_{max} of 1.9 pmol per mg protein for FaDu cells were obtained for **[^{64}Cu]Cu-(NOTA)$_3$-C225-Cys-c-PNA**. **[^{64}Cu]Cu-(NOTA)$_3$-C225** showed slightly different dissociation constants with a K_d of 7.7 ± 0.8 nM and B_{max} of 15.9 pmol per mg protein for A431 and a K_d of 2.0 ± 0.3 nM and B_{max} of 2.9 pmol per mg protein for FaDu cells. Modification of the monoclonal antibody with PNAs does not affect its binding behavior to EGFR expressing tumor cells. This is of particular importance since the immunoreactivity as well

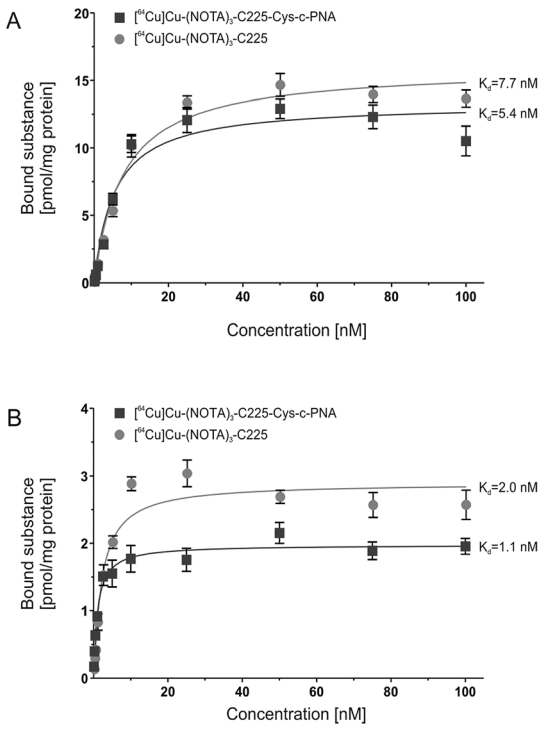

Fig. 1 *In vitro* binding studies of radiolabeled cetuximab conjugates. Saturation curves of [^{64}Cu]Cu-(NOTA)$_3$-C225-Cys-c-PNA and [^{64}Cu]Cu-(NOTA)$_3$-C225 upon incubation with human EGFR-positive tumor cell lines A431 (A) and FaDu (B).

Table 3 *In vitro* binding characteristics of radiolabeled cetuximab conjugates to human EGFR-positive tumor cells

Cell line		[^{64}Cu]Cu-(NOTA)$_3$-C225-Cys-c-PNA	[^{64}Cu]Cu-(NOTA)$_3$-C225
A431	K_d	5.4 ± 0.9 nM	7.7 ± 0.8 nM
	B_{max}	13.3 ± 0.6 pmol mg^{-1}	15.9 ± 0.4 pmol mg^{-1}
FaDu	K_d	1.1 ± 0.2 nM	2.0 ± 0.3 nM
	B_{max}	1.9 ± 0.1 pmol mg^{-1}	2.9 ± 0.1 pmol mg^{-1}

as the high affinity of cetuximab to EGFR has to be conserved after chemical conjugation.[56]

The variation in the affinity of the antibody conjugates between A431 and FaDu cells can be explained by the different cellular context. Such an effect has been previously reported for EGF.[97] Björkelund and co-workers indeed observed an important influence of the investigated cell lines on the binding characteristics and on the multiple ligand–receptor interactions. The authors explained these phenomena by the occurrence of varying ratios of EGFR homodimers and heterodimers composed of EGFR and the human epidermal growth factor receptor 2 (HER2) due to different expression levels of these receptors. The different ratios of EGFR and HER2 may also account for the herein described variation in the affinity of the cetuximab conjugates between A431 and FaDu cells. The former cell line overexpresses EGFR with 1–3 × 10^6 receptors per cell[98] and has a lower HER2 expression,[96,99,100] whereas the latter cell line possesses a large HER2 population and presents less EGFR on the cell surface (7 × 10^5 receptors per cell).[96,99,101]

Biodistribution studies

The data previously presented by Hnatowich and co-workers[32–34,49] and by our laboratories[48] demonstrated favorable properties of radiolabeled PNAs towards *in vivo* tumor pretargeting applications. These include very fast distribution, low non-specific accumulation in non-targeted tissue as well as renal elimination as preferred elimination pathway from organism. However, these experiments also showed that specific accumulation of radiolabeled PNA derivatives in pretargeted tumor tissue might not be sufficiently high for therapeutic approaches.[33,34,49] The reason behind it is certainly the rapid elimination of the radiolabeled PNA from blood. The major aim of attaching large PEG moieties onto our 17-mer PNA oligomers was therefore to increase blood retention and subsequently enhance blood availability. This should result into increased hybridization incidences in pretargeted tumor tissue.

As an initial step of this evaluation process, we determined the impact of the degree of PEGylation on the radiopharmacological behavior by conducting biodistribution studies and dynamic SPECT scans in healthy male Wistar rats. To ensure comparability and compatibility with further animal studies as well as published results, the data presented are the means ± standard deviation of standard uptake values (SUV), defined as the tracer concentration at a certain time point normalized to injected dose per unit body weight. Detailed biodistribution data presented as SUV and %ID are summarized in Tables S2 and S3.† At 5 min post injection (Table 4), the ^{99m}Tc-labeled 17-mer PNA conjugates clearly showed an elevated level of activity concentration in the blood pool with increasing degree of PEGylation. Compared to the non-PEGylated 17-mer **Dpa-PNA**, the attachment of PEG led to about 10% and 45% higher activity concentration in the blood pool for 2 kDa PEG and 10 kDa PEG, respectively.

In agreement with the concept of tumor pretargeting,[102] all radiolabeled PNA conjugates were distributed by the blood stream very rapidly and were almost completely eliminated from the blood pool 60 min after administration. This

Table 4 Biodistribution data for ^{99m}Tc-labeled PNA derivatives performed in healthy male Wistar rats at 5 min and 60 min after single intravenous injection. Data are presented as SUV

	17-mer [^{99m}Tc](Tc-Dpa)-PNA		17-mer [^{99m}Tc](Tc-Dpa)-(Cys-PEG$_{2kDa}$)-PNA		17-mer [^{99m}Tc](Tc-Dpa)-(Cys-PEG$_{10kDa}$)-PNA	
	5 min p.i. (n = 12)	60 min p.i. (n = 11)	5 min p.i. (n = 8)	60 min p.i. (n = 8)	5 min p.i. (n = 8)	60 min p.i. (n = 8)
Blood	1.36 ± 0.21	0.24 ± 0.10	1.51 ± 0.13	0.24 ± 0.06	2.01 ± 0.38	0.34 ± 0.11
Kidneys	11.7 ± 1.60	13.1 ± 1.99	12.0 ± 1.42	9.29 ± 1.10	11.3 ± 1.86	9.75 ± 2.64
Adrenals	0.56 ± 0.12	0.14 ± 0.04	0.80 ± 0.25	0.32 ± 0.21	0.82 ± 0.15	0.25 ± 0.08
Liver	0.91 ± 0.23	0.85 ± 0.26	1.12 ± 0.42	0.98 ± 0.42	1.15 ± 0.21	0.73 ± 0.30
Spleen	0.59 ± 0.31	0.22 ± 0.04	0.92 ± 0.29	0.71 ± 0.34	0.60 ± 0.13	0.54 ± 0.46
Pancreas	0.51 ± 0.30	0.14 ± 0.16	0.35 ± 0.04	0.26 ± 0.25	0.51 ± 0.06	0.61 ± 1.24
Thymus	0.46 ± 0.09	0.10 ± 0.02	0.46 ± 0.08	0.10 ± 0.01	0.45 ± 0.06	0.12 ± 0.04
Muscles	0.38 ± 0.16	0.05 ± 0.01	0.35 ± 0.03	0.09 ± 0.04	0.30 ± 0.08	0.13 ± 0.09
Lung	1.06 ± 0.18	0.22 ± 0.06	2.30 ± 0.69	2.16 ± 1.36	1.41 ± 0.24	0.42 ± 0.16
Heart	0.58 ± 0.07	0.10 ± 0.04	0.64 ± 0.06	0.13 ± 0.04	0.81 ± 0.21	0.17 ± 0.06
Femur	0.56 ± 0.03	0.16 ± 0.02	0.45 ± 0.01	0.14 ± 0.03	0.51 ± 0.07	0.16 ± 0.04
Testicles	0.25 ± 0.13	0.09 ± 0.02	0.34 ± 0.14	0.13 ± 0.03	0.34 ± 0.08	0.16 ± 0.03
Hadrian glands	0.57 ± 0.08	0.12 ± 0.03	0.58 ± 0.18	0.18 ± 0.15	0.59 ± 0.09	0.17 ± 0.04
Brain	0.04 ± 0.01	0.01 ± 0.00	0.04 ± 0.00	0.02 ± 0.02	0.07 ± 0.02	0.01 ± 0.01
Hair & Skin	0.79 ± 0.07	0.24 ± 0.11	0.93 ± 0.08	0.24 ± 0.03	0.86 ± 0.19	0.28 ± 0.07

Table 5 Comparison of ^{99m}Tc activity concentration of radiolabeled 17-mer PNA conjugates of current studies with previously published 12-mer PNA[48] in healthy male Wistar rats at 5 min and 60 min after single intravenous injection. Data are presented as SUV

	12-mer [^{99m}Tc]-(Tc-Dpa)-PNA from ref. 48	17-mer [^{99m}Tc]-(Tc-Dpa)-PNA	17-mer [^{99m}Tc](Tc-Dpa)-(Cys-PEG$_{2kDa}$)-PNA	17-mer [^{99m}Tc](Tc-Dpa)-(Cys-PEG$_{10kDa}$)-PNA
Blood 5 min p.i. (60 min p.i.)	1.21 ± 0.05 (0.26 ± 0.10)	1.36 ± 0.21 (0.24 ± 0.10)	1.51 ± 0.13 (0.24 ± 0.06)	2.01 ± 0.38 (0.34 ± 0.11)
Kidneys 5 min p.i. (60 min p.i.)	7.12 ± 0.43 (5.45 ± 0.45)	11.7 ± 1.60 (13.11 ± 1.99)	12.0 ± 1.42 (9.29 ± 1.10)	11.3 ± 1.86 (9.75 ± 2.64)
Liver 5 min p.i. (60 min p.i.)	0.99 ± 0.03 (0.67 ± 0.10)	0.91 ± 0.23 (0.85 ± 0.26)	1.12 ± 0.42 (0.98 ± 0.42)	1.15 ± 0.21 (0.73 ± 0.30)

minimizes unpredictable whole-body radiation exposure. As expected for compounds with molecular weights significantly lower than 30 kDa and of highly hydrophilic nature (see log $D_{o/w}$ values from Table 2), the activity was almost exclusively eliminated *via* the renal pathway.

Compared with previously published results on a 12-mer PNA conjugate **[^{99m}Tc](Tc-Dpa-PNA)**,[48] the expansion to a 17-mer conjugate enhanced blood availability 5 min p.i. by about 12% (Table 5).

In combination with the attachment of a PEG moiety, we were able to further elevate blood availability to 25% and 66% for 2 kDa PEG and 10 kDa PEG, respectively. The increase in the length of the PNA sequence from 12-mer to 17-mer also led to higher kidney uptake from (7.12 ± 0.43) SUV to (11.71 ± 1.60) SUV and (5.45 ± 0.45) SUV to (13.11 ± 1.99) SUV 5 min and 60 min post injection, respectively. Similar relationship between the length of oligonucleotide sequence and kidney retention has been reported for morpholino-type oligonucleotides[92] and has also been observed, in a much greater extent, for L-configured DNA-oligonucleotides in our laboratories.[83]

Based on compiled data (see Fig. 2), among the 17-mer PNA conjugates used in this study, **[^{99m}Tc](Tc-Dpa)-(Cys-PEG$_{10kDa}$)-PNA** exhibits the highest activity concentration in the blood pool and the lowest activity concentration in liver and kidney tissue (60 min p.i.) combined with a trend of wash-out from those organs. This promising 17-mer PNA conjugate was therefore further evaluated by dynamic SPECT scans.

SPECT image 5 min post injection (Fig. 3) substantiated an almost homogeneous blood distribution with enhanced activity concentration in heart, left and right carotids, both kidneys with hotspots at the renal pelvis, and bladder (urine). As demonstrated with the SPECT images at 60 min post injection, the majority of activity has been eliminated from blood pool *via* kidneys into the bladder. The calculated activity-under-curve (AUC) projection clearly shows removal of activity by renal pathway.

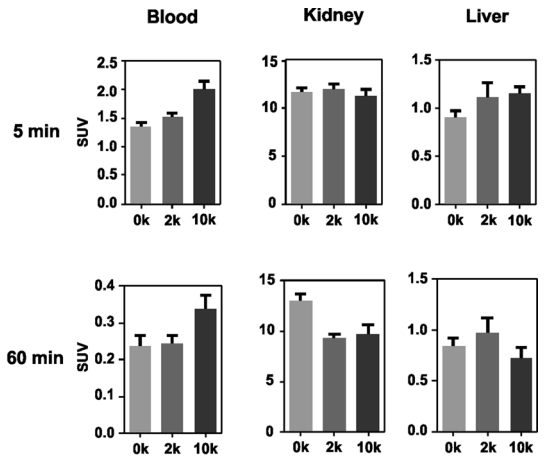

Fig. 2 Comparison of activity concentration (SUV) in the blood, kidneys and liver of rats after single intravenous injection following sacrifice at 5 and 60 min p.i.

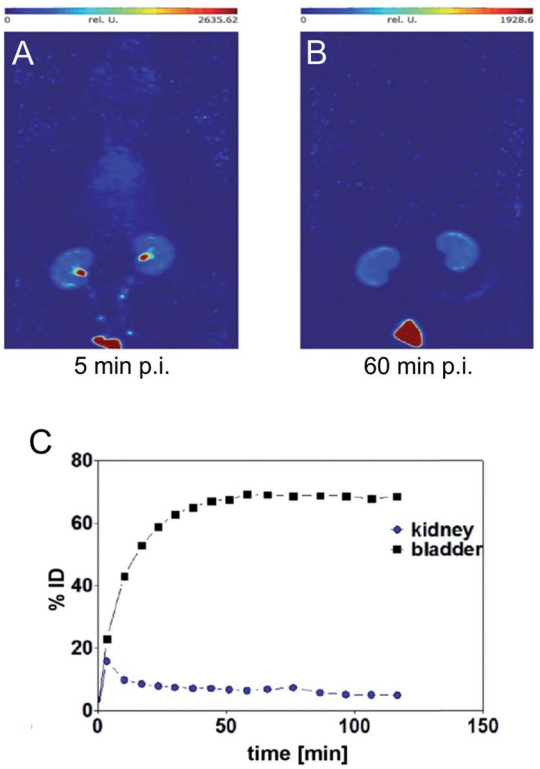

Fig. 3 Maximum intensity projections generated from dynamic SPECT (A and B) and calculated activity-under-curve for bladder and kidney tissue of [^{99m}Tc](Tc-Dpa)-(Cys-PEG$_{10kDa}$)-PNA (C) after single intravenous administration in single healthy male Wistar rat (SPECT/CT images and tumor mouse are presented in Fig. S18†).

Radio-HPLC analysis of **[^{99m}Tc](Tc-Dpa)-(Cys-PEG$_{10kDa}$)-PNA** samples from rat arterial blood, kidney extracts and urine showed no metabolic degradation over a time period of 120 min post injection (Fig. S17†).

Evaluation of the pretargeting approach

These promising radiopharmaceutical results strongly encouraged us to investigate the tumor pretargeting approach using **Dpa-(Cys-PEG$_{10kDa}$)-PNA**. Tumor xenografts (epidermoid carcinoma) were obtained after subcutaneous injection of A431 cells into the right thigh of female NMRI nu/nu mice. Imaging and biodistribution studies were performed when the tumor were in the range of 8 to 13 mm.

The control experiment in this xenograft model without pretreatment of **(NOTA)$_3$-C225-Cys-c-PNA** before injection of **[^{99m}Tc](Tc-Dpa)-(Cys-PEG$_{10kDa}$)-PNA** showed no radioactivity localization in tumor site (Fig. 4A). The remaining radioactivity after 1 h p.i. is mainly located in the kidneys as expected on the basis of biodistribution experiments with rats described above.

When mice were pretreated with **(NOTA)$_3$-C225-Cys-c-PNA** 24 h prior to administration of **[^{99m}Tc](Tc-Dpa)-(Cys-PEG$_{10kDa}$)-PNA**, SPECT images clearly demonstrated an accumulation of radioactivity at tumor site referring to efficient and rapid *in vivo* hybridization at pretargeted tumor tissue. The tumor is clearly visible after 60 min (Fig. 4B) and the radioactivity can be detected for at least 1 day (Fig. 4C). The enhanced radioactivity level in the kidneys, liver and blood compared to the control experiment is due to the circulating antibody conjugate. The activity wash-out from blood and tissues is faster relative to the tumor. Altogether, the tumor pretargeting using PNA allows for fast tumor localization and can be considered for improved *in vivo* targeting.

For more detailed evaluation of our pretargeting approach, we also conducted biodistribution studies in eight murine xenografts, applying the same experimental conditions as described for SPECT imaging (single intravenous injection of **(NOTA)$_3$-C225-Cys-c-PNA** 24 h prior to administration of **[^{99m}Tc](Tc-Dpa)-(Cys-PEG$_{10kDa}$)-PNA**). 24 h post injection of **[^{99m}Tc](Tc-Dpa)-(Cys-PEG$_{10kDa}$)-PNA**, an enhanced radioactivity concentration of SUV 0.63 ± 0.27 was determined in tumor tissue (Fig. 5). Compared with non-targeted muscle tissue, a high contrast of tumor-to-muscle ratio of 8.29 ± 1.28 was achieved. The elevated levels of activity concentration in blood, liver, heart, and lung may be explained by incomplete blood elimination of **(NOTA)$_3$-C225-Cys-c-PNA**. It is very likely that circulating **(NOTA)$_3$-C225-Cys-c-PNA** formed hybrids with **[^{99m}Tc](Tc-Dpa)-(Cys-PEG$_{10kDa}$)-PNA** in blood pool leading to enhanced retention time of activity in blood and aforementioned organs. This is in agreements with findings for PNA–streptavidin conjugates circulating in the blood to be able to efficiently bound radiolabeled complementary PNA.[33]

Although a distinct accumulation of activity in the tumor site was observed 60 min after the administration of radiolabeled complementary PNAs to pretargeted mice, the resulting tumor-to-blood ratios might not be ideal. We determined that the waiting period of 24 h between both administrations represented the optimal balance in terms of rate of blood clearance and rate of internalization of PNA–cetuximab conjugates. On one hand, extended intervals such as 72 h would enhance blood clearance of the antibody–PNA conjugates as well as decrease activity concentration in blood, liver, heart, and lung. On the other hand, PNA–cetuximab conjugates bound to EGF-receptors are undergoing internalization *via* receptor-mediated endocytosis, which gradually diminishes the amount of hybridization events with radiolabeled complementary PNAs. For this reason, we believe that extended waiting will not significantly enhance tumor-to-background ratios.

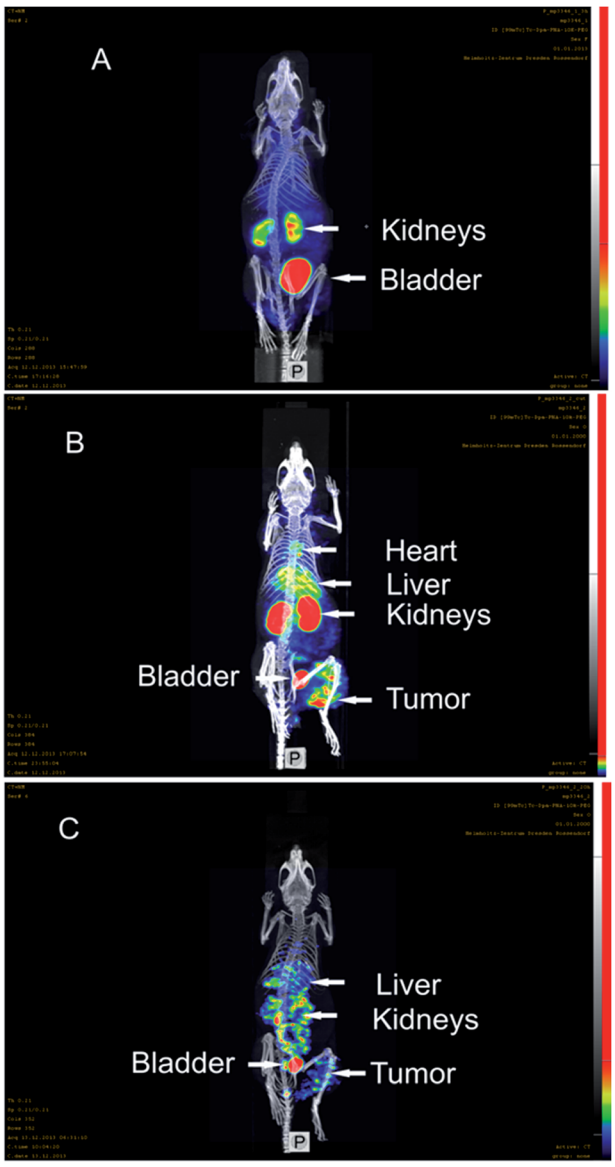

Fig. 4 SPECT/CT maximum intensity projection images of [^{99m}Tc](Tc-Dpa)-(Cys-PEG$_{10kDa}$)-PNA in murine A431 tumor xenograft (NMRI nu/nu mice; tumor located at right thigh). (A) 1 h post injection of [^{99m}Tc](Tc-Dpa)-(Cys-PEG$_{10kDa}$)-PNA without preinjection of (NOTA)3-C225-Cys-c-PNA. (B) 1 h post injection of radiotracer; (NOTA)$_3$-C225-Cys-c-PNA was administered 24 h before injection of radiotracer. (C) 20 h post injection of radiotracer; (NOTA)$_3$-C225-Cys-c-PNA was administered 24 h before injection of radiotracer.

Blood	1.42 ± 0.75
Kidneys	0.48 ± 0.16
Adrenals	0.32 ± 0.14
Liver	2.18 ± 0.11
Spleen	0.42 ± 0.12
Pancreas	0.18 ± 0.10
Muscles	0.08 ± 0.03
Lung	0.55 ± 0.26
Heart	0.36 ± 0.24
Femur	0.11 ± 0.05
Brain	0.05 ± 0.03
Tumor	0.63 ± 0.27
Tumor/Muscle	**8.29 ± 1.28**
Tumor/Blood	**0.48 ± 0.09**

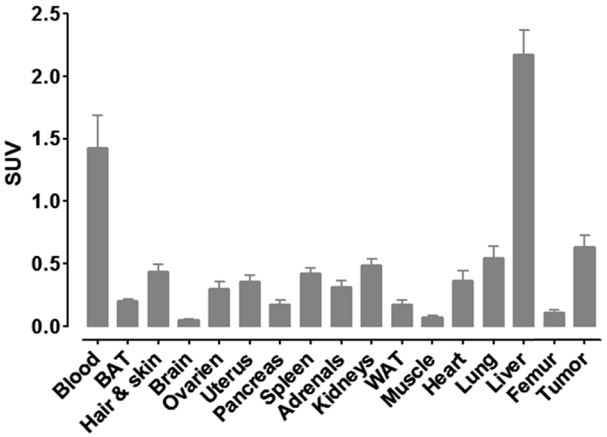

Fig. 5 Biodistribution of [^{99m}Tc](Tc-Dpa)-(Cys-PEG$_{10kDa}$)-PNA (24 h post injection of radiotracer) in murine xenograft (NMRI nu/nu mice; A431 tumor cells transplanted into right thigh) 24 h after single administration of (NOTA)$_3$-C225-Cys-c-PNA. Values in the table are averages in SUV including standard deviation (8 mice).

Conclusions

The search for novel radiotheragnostic modalities for the detection and treatment of cancer is currently attracting a lot of attention worldwide. Among the different options investigated, the use of a pretargeting approach with the non-natural DNA/RNA analogues Peptide Nucleic Acids (PNAs) as recognition units is extremely attractive.[33] By temporally separated administration of the antibody–PNA conjugate and its radiolabeled complementary PNA counterpart, the important limitations of conventional directly radiolabeled antibodies are overcome. Among these limitations, slow blood clearance has been identified as a major hurdle for diagnostic tumor discrimination, requiring extensive waiting times, which can last up to a week after administration before image acquisition. Furthermore, mAb accumulation in non-target tissues results in radiation damage to non-tumor cells and subsequently in severe toxicity.[8] The herein exemplified pretargeting approach using PNAs facilitates the rational use of mAb conjugates for diagnostic and therapeutic purposes since it allows for sufficient time for the antibody–PNA conjugate to find the target tissue and for the rapid clearance of the radioactive PNA construct from circulation and normal tissues.

By eliminating the hitherto existing limitations of PNAs such as insufficient water solubility as well as unfavorable biodistribution,[41] we successfully optimized this complementary system for future pretargeting approaches. Nonetheless, the herein obtained results for our PNA-based approach cannot be juxtaposed with reported studies applying phosphorodiamidate morpholino oligomers (MORFs) due to major divergences with respect to animal models, tumor entities as well as tumor cell-related molecular targets and corresponding antibodies. Neglecting these facts, similar tumor uptake and non-target ratios were achieved.[28,31] All in all, as demonstrated in this article, PNAs are a favorable alternative to MORFs for this field of research, especially when considering their relatively facile synthesis.

More specifically, in this article, we initially described the first detailed radiopharmaceutical evaluation of PNA bioconjugates for tumor pretargeting. We could then demonstrate that the PEGylation of PNA oligomers resulted into optimized pharmacokinetic properties. Compared with their non-PEGylated analogue, PEGylated PNAs showed lower kidney and liver accumulation, better renal excretion and a more beneficial residence time in blood. We also present a versatile conjugation protocol to modify the EGFR specific therapeutic antibody cetuximab. Coupling of a cysteine-functionalized PNA oligomer to the mAb equipped with maleimido functional groups was achieved at ambient temperature. As expected, under these conditions, the modification of cetuximab with the PNA conjugate did not affect its binding properties towards EGFR-positive tumor cells showing hence that this modified antibody could be used in our study. Very importantly, *in vivo* studies in tumor bearing mice demonstrated the high potential of the described pretargeting approach. Rapid and efficient *in vivo* hybridization of a fast-clearing radiolabeled complementary PNA with a cetuximab-PNA conjugate led to high specific tumor accumulation. The studies performed have shown that the 17-mer PNAs investigated are promising candidates for further preclinical studies. All in all, this study opens up new avenues not only in the field of radioimaging but also in the field of cancer radioimmunotherapy. We are currently analyzing if such an approach could be used to treat cancer by using therapeutic radionuclides such as ^{90}Y, ^{177}Lu, ^{186}Re or ^{188}Re.

Experimental section

Material and methods

Chemicals and solvents were of reagent grade or better and purchased from commercial suppliers and were used without

further purification unless otherwise specified. Alpha-methoxy-omega-ethyl-maleimide poly(ethylene glycol) (MeO-PEG-mal; MeO-PEG_{2kDa}-maleimide with PDI = 1.03; MeO-PEG_{10kDa}-maleimide with PDI = 1.08) and *N*-alpha-(9-fluorenylmethyloxycarbonyl)-*S*-trityl-L-cysteine (Fmoc-L-Cys(Trt)-OH) were purchased from Iris Biotech. PNA monomers were supplied by Link technologies. TentaGel S RAM Lys(Boc) Fmoc resin was purchased from Rapp Polymere. 2,2′-dipicolylamine (**Dpa-N_3**) was prepared following a previously reported procedure.[48] All other chemicals were of reagent-grade and sourced from Sigma-Aldrich.

ESI-MS spectra were recorded on a Bruker Esquire 6000. The matrix-assisted laser desorption/ionization time of flight mass spectrometry (MALDI-TOF) mass spectra were measured on a Bruker Daltonics Autoflex. The experiments were performed in reflector (RP) or linear (LP) mode with positive polarity using α-cyano-4-hydroxy-cinnamic acid on a Prespotted AnchorChip (PAC HCCA) or sinapinic acid (SA) as the matrix. LC-MS spectra were measured on an Acquity™ from Waters system equipped with a PDA detector and an auto sampler using an Agilent Zorbax 300SB-C18 analytical column (3.5 μm particle size, 300 Å pore size, 150 × 4.6 mm). This LC was coupled to an Esquire HCT from Bruker (Bremen, Germany) for the MS measurements. The LC run (flow rate: 0.3 mL min^{-1}) was performed with a linear gradient of A (distilled water containing 0.1% v/v formic acid) and B (acetonitrile (Sigma-Aldrich HPLC-grade), containing 0.1% v/v formic acid); $t = 0$ min, 5% B; $t = 3$ min, 5% B; $t = 17$ min, 100% B; $t = 20$ min, 100% B; $t = 25$ min, 5% B. HPLC purification was performed on a Varian ProStar system equipped with a UV/Vis spectrometer and an Agilent Zorbax 300SB-C18 prep column (5 μm particle size, 300 Å pore size, 150 × 21.1 mm. Flow rate: 20 mL min^{-1}). The runs were performed with a linear gradient of A (distilled water containing 0.1% v/v TFA) and B (acetonitrile (Sigma-Aldrich HPLC-grade), containing 0.1% v/v TFA). Preparative run: $t = 0$ min, 5% B; $t =$ 17 min, 42% B; $t = 25$ min, 100% B; $t = 30$ min, 100% B; $t =$ 32 min, 5% B (for **Dpa-PNA**, **Dpa-Cys-PNA** and **Cys-c-PNA**). Preparative runs: $t = 0$ min, 10% B; $t = 24$ min, 60% B; $t =$ 25 min, 100% B; $t = 30$ min, 100% B; $t = 32$ min, 10% B (for **Dpa-(Cys-PEG_x)-PNA**). The size exclusion purification was performed on an AKTAprime Plus system using HiTrap Desalting 5 × 5 mL GE Healthcare (10 mM HCl in distilled water, flow rate 3 mL min^{-1}). Radio-HPLC of the ^{99m}Tc labeled Dpa-PNA derivatives were performed on a Perkin-Elmer system with quaternary pump (series 200 LC pump) equipped with a radio-detector (RAMONA from raytest), a UV/Vis-detector (LC 290 from Perkin-Elmer) and an Eurosphere 100 column (5 μm particle size, 200 mm × 4.5 mm, flow rate: 1 mL min^{-1}). The runs were performed with a linear gradient of A (distilled water containing 0.1% v/v TFA) and B (acetonitrile Fisher HPLC-grade, containing 0.1% v/v TFA): $t = 0$ min, 0% B; $t = 20$ min, 100% B. Supernatants from samples of arterial blood plasma were analyzed on a Hewlett Packard system (series 1100) equipped with a radio-detector (RAMONA from raytest) and a Zorbax C18 300SB column (4 μm particle size, 9.4 × 250 mm, flow rate: 2 mL min^{-1}, column temperature 30 °C). The runs were performed with a linear gradient of A (50 mM aqueous triethylamine-acetic acid buffer pH = 6.45) and B (acetonitrile Fisher HPLC-grade): $t = 0$ min, 5% B, $t = 15$ min, 50% B, $t = 16$ min 95% B, $t = 20$ min, 95% B. Radio-TLC of the ^{64}Cu-labeled antibody conjugates **[^{64}Cu]Cu-(NOTA)$_3$-C225** and **[^{64}Cu]Cu-(NOTA)$_3$-C225-Cys-c-PNA** were performed at ITLC-SA plates and 0.9% sodium chloride solution as mobile phase. UV/Vis measurements and hybridization studies were performed on a Specord 210 from Analytik Jena AG. To determine the concentrations of PNA-derivatives measurements carried out at 260 nm by 90 °C with following extinction coefficients: **Cys-c-PNA** $\varepsilon = 197$ μL × $nmol^{-1}$ × cm^{-1}, **Dpa-PNA**, **Dpa-(Cys-PEG_{2kDa})-PNA**, and **Dpa-(Cys-PEG_{10kDa})-PNA** $\varepsilon = 182$ μL × $nmol^{-1}$ × cm^{-1}. Cetuximab derivatives were measured at 280 nm by room temperature. The extinction coefficient was determined *via* UV/Vis calibration curve and linear regression analysis: **C225** $\varepsilon = 217 \pm 14$ μL $nmol^{-1}$ cm^{-1}.

General chemistry

General procedure for synthesis of PNAs. The synthesis of the PNAs was performed as previously reported by our groups.[48] More specifically, the SPPS of PNAs was performed manually in 5 mL polypropylene one-way syringes equipped with a frit at the bottom. They were filled with 100 mg of polystyrene resin beads TentaGel S RAM Lys(Boc)Fmoc (0.23 mmol g^{-1}). The resin was swollen in DMF for 1 h before use. All reactions were performed on a mechanical shaker at 400 rpm with approximately 3–4 mL of freshly prepared solutions in the syringes. Fmoc/Bhoc-protected PNA monomers, the Fmoc spacer (5.0 equiv., all from Link Technologies, Lanarkshire, Scotland) or cysteine were preactivated in Eppendorf tubes before every coupling step for 2 min with HATU (4.5 equiv.) in DMF, adding DIPEA and 2,6-lutidine (10.0 equiv. each, 2 min for the T and G(Bhoc) PNA monomers and the PNA spacer, 5 min for the A(Bhoc)-PNA-monomer and 7 min for C(Bhoc)-PNA-monomer). For each coupling step the resin beads were treated with the activated acid under shaking for 1.5 h and subsequently washed with DMF. The coupling step was monitored by the Kaiser test. Two Fmoc deprotection steps were performed with piperidine (20%, v/v) in DMF (2 + 10 min). The resin beads were then washed successively with DMF, DCM and DMF. The whole procedure (deprotection, coupling, monitoring) was repeated for every PNA monomer until the PNA sequence was completed. Before cleavage, the resin was shrunk with methanol and dried. The PNAs were then cleaved using a mixture of trifluoroacetic acid–water–triisopropylsilane 95 : 2.5 : 5 v/v/v [3 × 1.5 mL (90 min each)]. The resulting solutions were first evaporated to dryness before being precipitated with ice-cold ether. The solids were centrifuged, washed with ice-cold ether and finally air-dried. The obtained crude oligomers were lyophilized in acetonitrile–water, purified and analyzed with RP-HPLC, and finally characterized with ESI and/or MALDI-TOF mass spectrometry.

Cys-c-PNA *(H-Cys-spacer-spacer-ataatcacataacataa-Lys-NH_2).* To obtain **Cys-c-PNA**, Fmoc-Cys(Trt)-OH was added to the growing PNA chain on the beads by using the same protocol as for PNA monomers (described above). The resulting **Cys-c-PNA** was cleaved off the resin following the general protocol shown above and purified by preparative HPLC to yield white powder.

Characterization: ESI-MS *m/z* 852.2 $[M + 6H]^{6+}$, 730.8 $[M + 7H]^{7+}$, 639.4 $[M + 8H]^{8+}$, 568.8 $[M + 9H]^{9+}$; MALDI-TOF (PAC HCCA, RP) *m/z* 5108.2 $[M + H]^{1+}$, 5130.2 $[M + Na]^{1+}$.

Dpa-PNA *(H-Dpa-spacer-spacer-ttatgttatgtgattat-Lys-NH_2).* To append the Dpa ligand to PNA, 4-pentynoic acid was added to the *N*-terminus of the PNA sequence according to the procedure previously reported by Gasser *et al.*[48] Dpa (5 equiv.) and CuI (2 equiv.) dissolved in a mixture DIPEA–DMF 1 : 6 v/v (4.207 mL) were introduced into the syringe and the mixture was shaken overnight. The resin was thoroughly washed by DMF, DCM, ACN, EDTA 0.1 M, shaken in EDTA 0.1 M for 2 h (3×) and washed by ACN, DCM and DMF. The product was then cleaved off the resin (see the General procedure above) and isolated by preparative HPLC as white powder. Characterization: ESI-MS *m/z* 1085.2 $[M + 5H]^{5+}$, 906.6 $[M + 6H]^{6+}$, 775.5 $[M + 7H]^{7+}$, 678.7 $[M + 8H]^{8+}$, 603.4 $[M + 9H]^{9+}$; 1097.9 $[M + Cu+5H]^{5+}$, 915.3 $[M + Cu+6H]^{6+}$, 785.1 $[M + Cu+7H]^{7+}$, 686.6 $[M + Cu+8H]^{8+}$, 610.5 $[M + Cu + 9H]^{9+}$; 1066.8 $[M - py(CH)_2 + 5H]^{5+}$, 889.0 $[M - py(CH)_2 + 6H]^{6+}$, 762.3 $[M + -py(CH)_2 + 7H]^{7+}$, 667.1 $[M + -py(CH)_2 + 8H]^{8+}$, 593.1 $[M + -py(CH)_2 + 9H]^{9+}$. MALDI-TOF (SA, LP) *m/z* 5422.2 $[M + H]^{1+}$, 5444.2 $[M + Na]^{1+}$, 5485.9 $[M + Cu + H]^{1+}$, 5393.8 $[M - py(CH_2) + Cu + H]^{1+}$, 5330.2 $[M - py(CH_2) + H]^{1+}$.

Dpa-Cys-PNA *(H-Dpa-spacer-spacer-Cys-spacer-spacer-ttatgt-tatgtgattat-Lys-NH_2).* To allow PEG conjugation *via* Michael addition, cysteine residue was added to the PNA sequence as described above for **Cys-PNA**. Dpa ligand was introduced as specified above for **DPA-PNA**. The product was cleaved off the resin (see the General procedure) and purified by preparative HPLC to obtain white powder. Characterization: ESI-MS *m/z* 831.4 $[M + 7H]^{7+}$, 727.6 $[M + 8H]^{8+}$, 647.1 $[M + 9H]^{9+}$. MALDI-TOF (SA, LP) *m/z* 5815.9 $[M + H]^{1+}$, 5837.8 $[M + Na]^{1+}$, 5879.4 $[M + Cu + H]^{1+}$, 5787.2 $[M - py(CH_2) + Cu + H]^{1+}$, 5723.7 $[M - py(CH_2) + H]^{1+}$, 5745.7 $[M - py(CH_2) + Na]^{1+}$.

Dpa-(Cys-PEG_x)-PNA. **Dpa-Cys-PNA** and TCEP (10 equiv.) were dissolved in distilled water (30 mL) and shaken overnight. The reaction mixture was then lyophilized, redissolved in 10 mM HCl and separated by size exclusion. The collected **Dpa-Cys-PNA** fractions were combined and split into two flasks (~20 mL each). MeO-PEG_{2kDa}-maleimide (5 equiv.) or MeO-PEG_{10kDa}-Maleimide (5 equiv.) was added and the mixture was then shaken overnight. The reaction mixtures were lyophilized, purified and analyzed with RP-HPLC and characterized by ESI and MALDI-TOF mass spectrometry.

Characterization of Dpa-(Cys-PEG_{2kDa})-PNA. MALDI-TOF (PAC HCCA, LP): a Gaussian distribution of peaks corresponding to PEG of various lengths (PEG_{35} to PEG_{45}) was observed; some of the most intense peaks: **Dpa-PEG_{42}-PNA** *m/z* 7822.2 $[M + H]^{1+}$, **Dpa-PEG_{43}-PNA** *m/z* 7866.2 $[M + H]^{1+}$, **Dpa-PEG_{44}-PNA** *m/z* 7910.2 $[M + H]^{1+}$, **Dpa-PEG_{45}-PNA** *m/z* 7954.4 $[M + H]^{1+}$, **Dpa-PEG_{46}-PNA** *m/z* 7998.4 $[M + H]^{1+}$, **Dpa-PEG_{47}-PNA** *m/z* 8042.5 $[M + H]^{1+}$, **Dpa-PEG_{41}-PNA** *m/z* 7778.1 $[M + H]^{1+}$, **Dpa-PEG_{40}-PNA** *m/z* 7734.0 $[M + H]^{1+}$, **Dpa-PEG_{39}-PNA** *m/z* 7690.0 $[M + H]^{1+}$, **Dpa-PEG_{38}-PNA** *m/z* 7645.9 $[M + H]^{1+}$, **Dpa-PEG_{37}-PNA** *m/z* 7601.9 $[M + H]^{1+}$. Corresponding $[M + 2H]^{2+}$ states, such as *m/z* 3911.6 **(Dpa-PEG_{42}-PNA)** were also observed.

Characterization of Dpa-(Cys-PEG_{10kDa})-PNA. MALDI-TOF (PAC HCCA, LP) a Gaussian distribution of peaks corresponding to PEG of various lengths (PEG_{230} to PEG_{270}) was observed; some of most intense peaks: **Dpa-PEG_{241}-PNA** *m/z* 16 588.1 $[M + H]^{1+}$, **Dpa-PEG_{242}-PNA** *m/z* 16 632.2 $[M + H]^{1+}$, **Dpa-PEG_{243}-PNA** *m/z* 16 676.2 $[M + H]^{1+}$, **Dpa-PEG_{244}-PNA** *m/z* 16 720.3 $[M + H]^{1+}$, **Dpa-PEG_{245}-PNA** *m/z* 16 764.3 $[M + H]^{1+}$, **Dpa-PEG_{246}-PNA** *m/z* 16 808.4 $[M + H]^{1+}$, **Dpa-PEG_{247}-PNA** *m/z* 16 852.4 $[M + H]^{1+}$, **Dpa-PEG_{248}-PNA** *m/z* 16 896.5 $[M + H]^{1+}$, **Dpa-PEG_{249}-PNA** *m/z* 16 940.1 $[M + H]^{1+}$, **Dpa-PEG_{250}-PNA** *m/z* 16 984.6 $[M + H]^{1+}$, **Dpa-PEG_{251}-PNA** *m/z* 17 028.6 $[M + H]^{1+}$, **Dpa-PEG_{252}-PNA** *m/z* 17 072.7 $[M + H]^{1+}$, **Dpa-PEG_{253}-PNA** *m/z* 17 116.7 $[M + H]^{1+}$, **Dpa-PEG_{254}-PNA** *m/z* 17 160.8 $[M + H]^{1+}$, **Dpa-PEG_{255}-PNA** *m/z* 17 204.8 $[M + H]^{1+}$, **Dpa-PEG_{256}-PNA** *m/z* 17 248.9 $[M + H]^{1+}$, **Dpa-PEG_{257}-PNA** *m/z* 17 292.9 $[M + H]^{1+}$, **Dpa-PEG_{258}-PNA** *m/z* 17 336.9 $[M + H]^{1+}$, **Dpa-PEG_{259}-PNA** *m/z* 17 381.0 $[M + H]^{1+}$, **Dpa-PEG_{260}-PNA** *m/z* 17 425.1 $[M + H]^{1+}$. Corresponding $[M + 2H]^{2+}$ states, such as *m/z* 8382.7 **(Dpa-PEG_{245}-PNA)** were also observed.

Polydispersity index (PDI) calculation for PEGylated PNAs. PDI index was calculated using the following formula:

$$\mathrm{PDI} = M_w/M_n$$

where M_w is weight average molecular weight defined as

$$M_w = \frac{\sum_i N_i M_i^2}{\sum_i N_i M_i}$$

and M_n is number average molecular weight defined as

$$M_w = \frac{\sum_i N_i M_i}{\sum_i N_i M_i}$$

where M_i is mass of a polymer of a certain length and N_i is the amount of this polymer present.

M_n and M_w were estimated from MALDI spectra. As PEG polymers used for synthesis had PDI <1.1 and PNA was monodisperse, PDI of PEGylated PNAs was expected to be <1.1. Therefore, no mass discrimination effect should have interfered, so N_i was assumed to be proportional to peak intensity in MALDI spectra. Calculated PDIs corresponded to those of PEG starting material.

Bioconjugation chemistry

$(NOTA)_3$-C225. 3 mL of Erbitux® stock solution (5 mg mL^{-1}) for infusion purposes were added to a Jumbosep™ centrifugal devices (30 kDa cut-off) containing 55 mL of 50 mM sodium bicarbonate saline buffer (pH 6.4). In order to completely remove infusion solution by sodium bicarbonate saline buffer, the procedure of centrifugal filtration was carried out 6 times (2500 min^{-1}, 60 min, 10 °C). The resulting Erbitux® solution (~6 mL) was finally concentrated to circa 1.2 mL by application of Macrosep™ Advance centrifugal device (30 kDa cut-off; 2500 min^{-1}, 90 min, 10 °C). The concentrated Erbitux® solution was transferred into a Teflon-coated plastic vial and 10.2 mg of *p*-SCN-Bn-NOTA × 3HCl (18.2 μmol) dissolved in 2.130 mL 50 mM HEPES buffer (pH 7.2) were added in aliquots. The

molar ration of the NOTA derivative to Erbitux® was 185 : 1 with a resulting pH value of 6.9. The reaction mixture was left for 22 h at room temperature and the vial was swirled occasionally.

The reaction mixture was worked up by centrifugal filtration for 6 times (Jumbosep™ centrifugal devices; 30 kDa cut-off; 50 mM sodium bicarbonate saline buffer; pH 6.4; 2500 min^{-1}, 60 min, 10 °C). Finally, the product solution was further concentrated to circa 1.0 mL by Macrosep™ Advance centrifugal device (30 kDa cut-off; 2500 min^{-1}, 90 min, 10 °C). The recovery of the antibody was almost quantitatively (98% by UV/Vis measurement). This value was assumed as yield. MALDI-TOF (SA, LP): Gaussian distribution of peaks was observed; most intense peaks: *m/z* 154 106 $[M + H]^{1+}$, *m/z* 77 184 $[M + 2H]^{2+}$.

$(NOTA)_3$-C225-mal. A solution of 50 mM sodium bicarbonate saline (pH 6.4; 0.9% w/w NaCl) containing **$(NOTA)_3$-C225** (app. 95–100 nmol) was diluted with phosphate buffer (pH 6.2) to a final volume of 3.400 mL and 1000 nmol 4-maleimido-butyric acid *N*-succinimidyl ester (0.28 mg) in 50 μL DMSO were added. The reaction mixture was left for 5 h at room temperature and swirled occasionally. The resulting **$(NOTA)_3$-C225-mal** was subsequently purified by centrifugal filtration for 6 times (Jumbosep™ centrifugal devices; 30 kDa cut-off; phosphate buffer pH 6.4; 2500 min^{-1}, 60 min, 10 °C). Finally, the product solution was further concentrated to circa 2.0 mL by Macrosep™ Advance centrifugal device (30 kDa cut-off; 2500 min^{-1}, 160 min, 10 °C). The recovery of the antibody was 85% (UV/Vis measurement). This value was assumed as yield. MALDI-TOF (SA, LP): Gaussian distribution of peaks was observed; most intense peaks: *m/z* 155 477 $[M + H]^{1+}$, *m/z* 77 984 $[M + 2H]^{2+}$.

$(NOTA)_3$-C225-Cys-c-PNA. 960 nmol of **Cys-c-PNA** (5110 g mol^{-1}) were dissolved in a mixture of 1000 μL of phosphate buffer and 1000 μL DMSO. This solution was added in aliquots to a Teflon-coated plastic vial containing the previously concentrated 2 mL phosphate buffer of **$(NOTA)_3$-C225-mal**. The molar ratio of **Cys-c-PNA** derivative to **$(NOTA)_3$-C225-mal** was app. 11 : 1. The reaction mixture was left for 4 days at room temperature and the vial was swirled occasionally. The high viscosity of DMSO containing solution led to extraordinary slow centrifugal filtration (Macrosep™ Advance device, 30 kDa cut-off). The addition of 12 mL phosphate buffer was required to dilute the reaction mixture, which also led to precipitation of non-reacted **Cys-c-PNA**. Subsequently, the solution was transferred into several *Protein low-bind tubes* from Eppendorf, cooled to 10 °C for 2 h, and centrifuged for 60 min (2500 min^{-1}, 10 °C). The resulting clear supernatant was transferred carefully into a Jumbosep™ device. After adding 40 mL of phosphate buffer the diluted reaction mixture was purified by centrifugal filtration. The purification using Jumbosep™ devices was performed 6 times. Finally, the product solution was further concentrated to circa 1.0 mL by Macrosep™ Advance centrifugal device (30 kDa cut-off; 2500 min^{-1}, 90 min, 10 °C). MALDI-TOF (SA, LP): Gaussian distribution of peaks was observed; most intense peaks: *m/z* 168 614.1 $[M + H]^{1+}$, *m/z* 86 022 $[M + 2H]^{2+}$.

The number of bound **Cys-c-PNA** to cetuximab was also spectrophotometrically determined by measuring the absorbance at different wavelengths.[92–94] The maximum absorbance of cetuximab was found to be at 280 nm and of **Cys-c-PNA** at 260 nm. Assuming that the conjugation of **Cys-c-PNA** to cetuximab will not influence the extinction coefficients of the individual compounds Lambert–Beer law were formulated at 260 nm and 280 nm. The extinction coefficients of cetuximab and Cys-c-PNA were determined *via* UV/Vis calibration curves and linear regression analysis: $\varepsilon_{\text{cetuximab 280 nm}} = 217 \pm 14$ μL $nmol^{-1}$ cm^{-1}, $\varepsilon_{\text{cetuximab 260 nm}} = 97 \pm 6$ μL $nmol^{-1}$ cm^{-1}, $\varepsilon_{\text{Cys-c-PNA 280 nm}} = 114 \pm 4$ μL $nmol^{-1}$ cm^{-1} and $\varepsilon_{\text{Cys-c-PNA 260 nm}} = 192 \pm 6$ μL $nmol^{-1}$ cm^{-1}. Based on the 260 nm/280 nm absorbance ratio, the conjugation degree can be calculated with following equation:

$$n = \frac{E_{280\text{ nm}} \times \varepsilon_{\text{C225 260 nm}} - E_{260\text{ nm}} \times \varepsilon_{\text{C225 280 nm}}}{E_{260\text{ nm}} \times \varepsilon_{\text{Cys-c-PNA 280 nm}} - E_{280\text{ nm}} \times \varepsilon_{\text{Cys-c-PNA 260 nm}}}$$

Radiochemistry

^{99m}Tc-labeling. 1.5–2.5 mL of freshly eluted $[^{99m}Tc]TcO_4^-$ solution (400–1450 MBq) were injected into IsoLink® vial. The resulting mixture was heated to 100 °C for 30 min. In order to prevent pressure issues and to concentrate the resulting $[^{99m}Tc]Tc(CO)_3(H_2O)_3^+$ solution, a syringe needle was inserted through the rubber plug of the vial. The needle was removed before the mixture was cooled to room temperature.

For each radiolabeling experiment 10 nmol of particular Dpa-PNA derivative from stock solution diluted in 400 μL of phosphate buffer (pH 5.4) were used. The labeling tube containing the PNA solution was gently flushed with argon for 5 min. Subsequently, approximately 400 μL $[^{99m}Tc]Tc(CO)_3(H_2O)_3^+$ kit solution (250–580 MBq) were added. The pH value of the radiolabeling mixture was tested by a triple zone pH-paper (*Tritest pH 1–11*). Optimal pH for radiolabeling ranges from 7 to 8. Occasionally, the pH value had to be adjusted by addition of further phosphate buffer (pH 5.4 or 8.2). The mixture was heated to 70 °C for 40 min and cooled to room temperature. The radiochemical yield (rcy) was determined by radio-HPLC. For HPLC injection purposes, 10 μL of labeling mixture were added to 90 μL of HPLC solvent A. For all radiolabeling experiments rcy of >95% determined from reaction mixtures ($n = 19$) were obtained. Decay corrected effective specific activities of up to 58 GBq μmol^{-1} were achieved. For *in vivo* studies (biodistribution and SPECT imaging) the radiolabeling mixtures were concentrated and re-buffered (sterile PBS) by centrifugal filtration (13 200 min^{-1}; 20 min; 25 °C; recovery of activity 70–80%). Centrifugal filtration was applied for purification purposes, if insufficient rcy (<95%) occurred. A typical volume of radiolabeled Dpa-PNA derivatives was 150–250 μL sterile phosphate buffered saline (PBS). Characterization: Radio-HPLC t_R: $^{99m}TcO_4^-$ 3.0 min; $[^{99m}Tc(H_2O)_3(CO)_3]^+$ 5.0–6.0 min; **Dpa-PNA** 10.5 min; **Dpa-(Cys-PEG_{2kDa})-PNA** 12.0 min; **Dpa-(Cys-PEG_{10kDa})-PNA** 12.9 min.

^{64}Cu-labeling. 3 nmol of antibody stock solution of **$(NOTA)_3$-C225** and **$(NOTA)_3$-C225-Cys-c-PNA**, resp., were diluted in 200 μL MES buffer (1 M, pH = 6.0). 50 MBq aliquots of $[^{64}Cu]$

$CuCl_2$ dissolved in 0.01 M HCl were added to 200 μL MES buffer (1 M, pH = 6.0) and then mixed with the antibody solution. The reaction mixture was incubated in a thermomixer for 35 min at 30 °C and the vial was swirled occasionally by manual stimulation. Afterwards, 4 μL of an aqueous EDTA solution (0.75 mM) were added to remove non-specific bound ^{64}Cu. After a reaction time of 10 min at room temperature the product mixture was checked by radio TLC for complete complexation of $[^{64}Cu]Cu^{2+}$. Rcy of >99% were achieved without any further purification (radiochemical purity >99%). **$[^{64}Cu]$Cu-(NOTA)$_3$-C225** and **$[^{64}Cu]$Cu-(NOTA)$_3$-C225-Cys-c-PNA** could be labeled with effective specific activities of up to 16.6 GBq μmol^{-1}. Characterization: Radio-TLC **$[^{64}Cu]$Cu-(NOTA)$_3$-C225** $R_f = 0$, **$[^{64}Cu]$Cu-(NOTA)$_3$-C225-Cys-c-PNA** $R_f = 0$.

Hybridization studies

Self-complementarity. UV/Vis cuvettes were filled with particular PNA probe at room temperature. After cooling to 5 °C the samples were heated to 95 °C.

Melting curves ($n = 2$). For hybridization studies equimolar amounts of 3 μM stock solutions of each **Dpa-PNA** derivatives and complementary **Cys-c-PNA** were filled into the cuvette. For the first step the single probes were heated up to 95 °C for 5 min to induce complete de-hybridization. The second step included cooling to 5 °C to achieve a fully hybridization with a gradient of 2 °C min^{-1}. During the third step the samples were heated with a gradient of 2 °C min^{-1} from 5 °C to 95 °C. The data points were analyzed with a polynomial fit (9th order) by the analysis software Origin Pro 8.6. The melting point T_M is equal to the maximum of the 1st differentiation of the sigmoid shaped melting curve.

Biological studies

Determination of log $D_{o/w}$ at 25 ± 1 °C. Information on the lipophilicity of ^{99m}Tc-labeled **Dpa-PNA**, **Dpa-(Cys-PEG$_{2kDa}$)-PNA** and **Dpa-(Cys-PEG$_{10kDa}$)-PNA** was obtained by distribution experiments in a water/1-octanol system. All radiolabeled PNA derivatives were isolated by HPLC in radiochemical purity of >98%. Aliquots of 250 kBq were added to phosphate buffered saline with pH values of 7.2, 7.4 and 7.6 reaching a total volume of 500 μL in 2 mL microcentrifuge tubes. To this solution, 500 μL of 1-octanol were added and the two phases were agitated in a thermomixer for 30 min at (25 ± 1) °C. After centrifugation of samples, aqueous and organic phases were separated and aliquots of both phases were measured using an automated gamma counter (PerkinElmer Life and Analytical Sciences). Each value was recorded as triplet.

Cell culture. For binding studies, two different adherent human tumor cell lines were used: the epidermoid carcinoma cell line A431 (ATCC® Number: CRL-1555) and the squamous cell carcinoma cell line FaDu (ATCC® number: HTB-43). All cells were cultured as previously reported.[87,103]

Binding affinity of $[^{64}Cu]$Cu-(NOTA)$_3$-C225-Cys-c-PNA and $[^{64}Cu]$Cu-(NOTA)$_3$-C225 to human EGFR-presenting cells. *In vitro* binding studies of **$[^{64}Cu]$Cu-(NOTA)$_3$-C225-Cys-c-PNA** and **$[^{64}Cu]$Cu-(NOTA)$_3$-C225** were performed as previously reported by Zarschler *et al.*[103] with slight modifications. Briefly, cells were plated in 24 well cell culture microplates (Greiner Bio-One) at a density of 1 × 10^5 cells per 0.5 mL per well and incubated for 48 h prior to addition of radiolabeled cetuximab conjugates. After 48 h, cells were preincubated for 30 min at 4 °C before the addition of different concentrations of radiolabeled cetuximab conjugates ranging from 0.1 nM to 100 nM. The cell culture microplates were further incubated for 60 min at 4 °C. Following treatment with radiolabeled cetuximab conjugates, cells were washed three times with PBS in order to ensure removal of loosely attached proteins from the cellular membrane. Finally, cell lysis was achieved by the addition of 1% SDS/0.1 M NaOH and incubation for 30 min at room temperature with vigorous shaking. The radioactivity in the cell extracts was quantified using an automated gamma counter (PerkinElmer Life and Analytical Sciences). Total protein concentration in cell extracts was determined colorimetrically with the *DC* Protein Assay (Bio-Rad Laboratories) according to the manufacture's microplate assay protocol using bovine serum albumin as protein standard.

Animal husbandry. The local animal research committee at the Landesdirektion Dresden approved the animal facilities and the experiments according to institutional guidelines and the German animal welfare regulations. Wistar rats (Wistar Unilever, HsdCpb: Wu, Harlan Winkelmann GmbH, Borchen, Germany) and mice (NMRI, nu/nu) were housed at 26 ± 2 °C. The received standard food and tap water *ad libitum*.

Biodistribution studies in Wistar rats and tumor mice. Wistar rats with a mean body weight 124 ± 25 g of 55 animals and female NMRI nu/nu tumor mice with a body weight 32 ± 2.5 g of 8 animals were used. Animals were anesthetized with desfluran (Suprane, Baxter, Unterschleißheim, Germany) initially with 10% in a 30% oxygen air mixture. The radiotracer (333 ± 66 kBq in 0.5 mL) was injected into a lateral tail vein and the animals were recovered. The injected dose was calculated from the activities of the syringes before and after the injection. After 5 and 60 min for rats and 24 h for tumor mice, animals were sacrificed under anesthesia. Blood was obtained by heart puncture and the organs and tissues of interest were removed and weighed and the radioactivity was determined using an automated NaI (Tl) well counter Wallac 1470 *Wizard* (Perkin Elmer Lifescience). The percentage of injected dose of organ (% ID) was calculated for organs that could be completely extracted and the standardized uptake value (SUV) was calculated according

$$\mathrm{SUV} = \frac{\text{tissue activity} \times \text{body weight}}{\text{injected activity} \times \text{tissue weight}} \quad (1)$$

The activity amounts in the urine were calculated as difference between the injected dose and the recovery from all individual organs, tissues, blood and carcass.

Metabolic profiling. To evaluate the kinetics and metabolism of **$[^{99m}$Tc](Tc-Dpa)-(Cys-PEG$_{10kDa}$)-PNA** in arterial rat blood, rats were anesthetized with desfluran and a catheter was set into the right femuralis. After radiotracer i.v. injection in a lateral tail vein were samples of arterial blood withdrawn and the blood

plasma was analyzed for **[^{99m}Tc](Tc-Dpa)-(Cys-PEG$_{10kDa}$)-PNA** content by radio-HPLC. The corresponding supernatants were analyzed by radio-HPLC.

SPECT of Wistar rats and tumor mice in pretargeting trial. Wistar rats (body weight 140 ± 51 g) were under desfluran anesthesia injected in a lateral tail vein with **[^{99m}Tc](Tc-Dpa)-(Cys-PEG$_{10kDa}$)-PNA** (58 MBq) and recovered. After one hour were the rats anesthetized, in the imaging bed positioned and in the NanoScanSPECT/CT imaged. CT was carried out in the NanoScan PET/CT. The DICOM image volume data were processed with InterView (Mediso, Budapest, Hungary) or converted to Siemens ECAT7 format for further processing with *Rover* software (ROI Visualization, Evaluation and Image Registration, *ABX Radeberg*, Germany). A431 human squamous carcinoma cells (Sigma Aldrich, 85090402-1VL) were subcutaneously inoculated in female NMRI nu/nu mice. 2×10^6 cells in 100 μL PBS were subcutaneously injected in the right thigh. Mice were studied when the tumors reached a size of 8 and 13 mm. The mice with A431 tumors were intravenously injected with 4 nmol **(NOTA)$_3$-C225-Cys-c-PNA**. At the next day, 45 MBq of **[^{99m}Tc](Tc-Dpa)-(Cys-PEG$_{10kDa}$)-PNA** were intravenously injected and imaged 1 h and 20 h later using NanoScan SPECT. CT was carried out in NanoScan PET/CT. The image processing was carried out as described above.

Statistics. The calculations and statistics were carried out with InterView (Mediso, Hungary), ROVER (ABX GmbH. Germany), R (A language and environment for statistical computing, R Foundation for Statistical Computing, Vienna, Austria. ISBN 3-900051-07-0, URL http://www.R-project.org.) and GraphPad Prism version 5.00 for Windows (GraphPad Software, San Diego California USA, http://www.graphpad.com).

Acknowledgements

We thank Karin Landrock for excellent technical assistance. This work was financially supported by the Swiss National Science Foundation (Professorships no. PP00P2_133568133568 and PP00P2PP00P2_157545157545 as well as Research Grants no. 200021_129910 and no. 200020_146776 to G.G), the University of Zurich (G.G), the Stiftung für Wissenschaftliche Forschung of the University of Zurich (G.G.), the Helmholtz Virtual Institute NanoTracking (Agreement no. VH-VI-421), the Research Department *Interfacial Systems Chemistry* at Ruhr University Bochum (N.M.-N.) and the COST Action CM1105 (N.M.-N and G.G.). This study is part of a research initiative Technologie und Medizin – Multimodale Bildgebung zur Aufklärung des *in-vivo*-Verhaltens von polymeren Biomaterialien of the Helmholtz-Portfoliothema.

References

1 J. Barbet, M. Bardies, M. Bourgeois, J. F. Chatal, M. Cherel, F. Davodeau, A. Faivre-Chauvet, J. F. Gestin and F. Kraeber-Bodere, *Methods Mol. Biol.*, 2012, **907**, 681–697.
2 I. Navarro-Teulon, C. Lozza, A. Pelegrin, E. Vives and J. P. Pouget, *Immunotherapy*, 2013, **5**, 467–487.
3 D. M. Goldenberg and R. M. Sharkey, *Expert Opin. Biol. Ther.*, 2012, **12**, 1173–1190.
4 R. K. Jain, *J. Natl. Cancer Inst.*, 1989, **81**, 570–576.
5 M. A. Tabrizi, C. M. Tseng and L. K. Roskos, *Drug Discovery Today*, 2006, **11**, 81–88.
6 S. M. Knowles and A. M. Wu, *J. Clin. Oncol.*, 2012, **30**, 3884–3892.
7 I. Vaneycken, M. D'Huyvetter, S. Hernot, J. De Vos, C. Xavier, N. Devoogdt, V. Caveliers and T. Lahoutte, *Curr. Opin. Biotechnol.*, 2011, **22**, 877–881.
8 P. Carter, *Nat. Rev. Cancer*, 2001, **1**, 118–129.
9 R. M. Sharkey and D. M. Goldenberg, *Immunotherapy*, 2011, **3**, 349–370.
10 S. J. Goldsmith, *Semin. Nucl. Med.*, 2010, **40**, 122–135.
11 F. Kyle and R. Pettengell, *Targeted Oncol.*, 2007, **2**, 173–179.
12 E. Frampas, C. Rousseau, C. Bodet-Milin, J. Barbet, J. F. Chatal and F. Kraeber-Bodere, *Front. Oncol.*, 2013, **3**, 159.
13 R. M. Sharkey, H. Karacay, T. M. Cardillo, C. H. Chang, W. J. McBride, E. A. Rossi, I. D. Horak and D. M. Goldenberg, *Clin. Cancer Res.*, 2005, **11**, 7109s–7121s.
14 D. M. Goldenberg, R. M. Sharkey, G. Paganelli, J. Barbet and J. F. Chatal, *J. Clin. Oncol.*, 2006, **24**, 823–834.
15 R. M. Sharkey, C. H. Chang, E. A. Rossi, W. J. McBride and D. M. Goldenberg, *Tumor Biol.*, 2012, **33**, 591–600.
16 D. J. Hnatowich, F. Virzi and M. Rusckowski, *J. Nucl. Med.*, 1987, **28**, 1294–1302.
17 S. J. Knox, M. L. Goris, M. Tempero, P. L. Weiden, L. Gentner, H. Breitz, G. P. Adams, D. Axworthy, S. Gaffigan, K. Bryan, D. R. Fisher, D. Colcher, I. D. Horak and L. M. Weiner, *Clin. Cancer Res.*, 2000, **6**, 406–414.
18 S. Shen, A. Forero, A. F. LoBuglio, H. Breitz, M. B. Khazaeli, D. R. Fisher, W. Wang and R. F. Meredith, *J. Nucl. Med.*, 2005, **46**, 642–651.
19 C. Grana, M. Chinol, C. Robertson, C. Mazzetta, M. Bartolomei, C. De Cicco, M. Fiorenza, M. Gatti, P. Caliceti and G. Paganelli, *Br. J. Cancer*, 2002, **86**, 207–212.
20 E. Gautherot, J. Bouhou, J. M. Le Doussal, C. Manetti, M. Martin, E. Rouvier and J. Barbet, *Cancer*, 1997, **80**, 2618–2623.
21 J. M. Le Doussal, A. Chetanneau, A. Gruaz-Guyon, M. Martin, E. Gautherot, P. A. Lehur, J. F. Chatal, M. Delaage and J. Barbet, *J. Nucl. Med.*, 1993, **34**, 1662–1671.
22 E. Janevik-Ivanovska, E. Gautherot, M. Hillairet de Boisferon, M. Cohen, G. Milhaud, A. Tartar, W. Rostene, J. Barbet and A. Gruaz-Guyon, *Bioconjugate Chem.*, 1997, **8**, 526–533.
23 R. M. Sharkey, W. J. McBride, H. Karacay, K. Chang, G. L. Griffiths, H. J. Hansen and D. M. Goldenberg, *Cancer Res.*, 2003, **63**, 354–363.
24 R. M. Sharkey, H. Karacay, W. J. McBride, E. A. Rossi, C. H. Chang and D. M. Goldenberg, *Clin. Cancer Res.*, 2007, **13**, 5577s–5585s.
25 F. Kraeber-Bodere, S. Bardet, C. A. Hoefnagel, M. R. Vieira, J. P. Vuillez, A. Murat, T. C. Ferreira, M. Bardies, L. Ferrer, I. Resche, E. Gautherot, E. Rouvier, J. Barbet and J. F. Chatal, *Clin. Cancer Res.*, 1999, **5**, 3190s–3198s.

26 F. Kraeber-Bodere, C. Rousseau, C. Bodet-Milin, L. Ferrer, A. Faivre-Chauvet, L. Campion, J. P. Vuillez, A. Devillers, C. H. Chang, D. M. Goldenberg, J. F. Chatal and J. Barbet, *J. Nucl. Med.*, 2006, **47**, 247–255.
27 R. Schoffelen, O. C. Boerman, D. M. Goldenberg, R. M. Sharkey, C. M. van Herpen, G. M. Franssen, W. J. McBride, C. H. Chang, E. A. Rossi, W. T. van der Graaf and W. J. Oyen, *Br. J. Cancer*, 2013, **109**, 934–942.
28 G. Liu, K. Mang'era, N. Liu, S. Gupta, M. Rusckowski and D. J. Hnatowich, *J. Nucl. Med.*, 2002, **43**, 384–391.
29 G. Liu, S. Dou, Y. Liu, Y. Wang, M. Rusckowski and D. J. Hnatowich, *Bioconjugate Chem.*, 2011, **22**, 2539–2545.
30 G. Liu, S. Dou, S. Baker, A. Akalin, D. Cheng, L. Chen, M. Rusckowski and D. J. Hnatowich, *Cancer Biol. Ther.*, 2010, **10**, 767–774.
31 G. Liu, C. Liu, S. Zhang, J. He, N. Liu, S. Gupta, M. Rusckowski and D. J. Hnatowich, *Nucl. Med. Commun.*, 2003, **24**, 697–705.
32 G. Mardirossian, K. Lei, M. Rusckowski, F. Chang, T. Qu, M. Egholm and D. J. Hnatowich, *J. Nucl. Med.*, 1997, **38**, 907–913.
33 M. Rusckowski, T. Qu, F. Chang and D. J. Hnatowich, *Cancer*, 1997, **80**, 2699–2705.
34 Y. Wang, F. Chang, Y. Zhang, N. Liu, G. Liu, S. Gupta, M. Rusckowski and D. J. Hnatowich, *Bioconjugate Chem.*, 2001, **12**, 807–816.
35 D. M. Goldenberg, C. H. Chang, E. A. Rossi, W. J. McBride and R. M. Sharkey, *Theranostics*, 2012, **2**, 523–540.
36 R. Rossin, S. M. van Duijnhoven, T. Lappchen, S. M. van den Bosch and M. S. Robillard, *Mol. Pharmaceutics*, 2014, **11**, 3090–3096.
37 T. Reiner and B. M. Zeglis, *J. Labelled Compd. Radiopharm.*, 2014, **57**, 285–290.
38 T. Reiner, J. S. Lewis and B. M. Zeglis, *J. Visualized Exp.*, 2015, e52335.
39 F. C. van de Watering, M. Rijpkema, M. Robillard, W. J. Oyen and O. C. Boerman, *Front. Med.*, 2014, **1**, 44.
40 J. Summerton and D. Weller, *Antisense Nucleic Acid Drug Dev.*, 1997, **7**, 187–195.
41 K. O. Mang'era, G. Liu, W. Yi, Y. Zhang, N. Liu, S. Gupta, M. Rusckowski and D. J. Hnatowich, *Eur. J. Nucl. Med. Mol. Imaging*, 2001, **28**, 1682–1689.
42 M. R. Lewis and F. Jia, *J. Cell. Biochem.*, 2003, **90**, 464–472.
43 S. Scarfi, M. Giovine, R. Pintus, E. Millo, E. Clavarino, M. Pozzolini, L. Sturla, R. P. Stock, U. Benatti and G. Damonte, *Biotechnol. Appl. Biochem.*, 2003, **38**, 61–69.
44 J. Segura, C. Fillat, D. Andreu, J. Llop, O. Millan, B. G. de la Torre, Z. Nikolovski, V. Gomez, N. Andreu, A. Pinyot, R. Castelo, J. D. Gispert and J. A. Pascual, *Ther. Drug Monit.*, 2007, **29**, 612–618.
45 Y. Shen, R. Shrestha, A. Ibricevic, S. P. Gunsten, M. J. Welch, K. L. Wooley, S. L. Brody, J. S. Taylor and Y. Liu, *Interface Focus*, 2013, **3**, 20120059.
46 C. Y. Shiue and S. Eck, in *Handbook of Radiopharmaceuticals*, ed. M. J. Welch and C. S. Redvanly, Wiley, New-York, USA, 2003, pp. 467–479.
47 X. Tian, M. R. Aruva, H. R. Wolfe, W. Qin, E. R. Sauter, M. L. Thakur, S. A. Waldman and E. Wickstrom, *Nucleosides, Nucleotides Nucleic Acids*, 2005, **24**, 1085–1091.
48 G. Gasser, K. Jäger, M. Zenker, R. Bergmann, J. Steinbach, H. Stephan and N. Metzler-Nolte, *J. Inorg. Biochem.*, 2010, **104**, 1133–1140.
49 F. Chang, T. Qu, M. Rusckowski and D. J. Hnatowich, *Appl. Radiat. Isot.*, 1999, **50**, 723–732.
50 I. Eke, M. Ingargiola, C. Förster, L. A. Kunz-Schughart, M. Baumann, R. Runge, R. Freudenberg, J. Kotzerke, J. M. Heldt, H. J. Pietzsch, J. Steinbach and N. Cordes, *Int. J. Radiat. Biol.*, 2014, **90**, 678–686.
51 M. Ingargiola, R. Runge, J. M. Heldt, R. Freudenberg, J. Steinbach, N. Cordes, M. Baumann, J. Kotzerke, G. Brockhoff and L. A. Kunz-Schughart, *Int. J. Cancer*, 2014, **135**, 968–980.
52 L. Koi, R. Bergmann, K. Brüchner, J. Pietzsch, H. J. Pietzsch, M. Krause, J. Steinbach, D. Zips and M. Baumann, *Radiother. Oncol.*, 2014, **110**, 362–369.
53 J. Saker, M. Kriegs, M. Zenker, J. M. Heldt, I. Eke, H. J. Pietzsch, R. Grenman, N. Cordes, C. Petersen, M. Baumann, J. Steinbach, E. Dikomey and U. Kasten-Pisula, *J. Nucl. Med.*, 2013, **54**, 416–423.
54 M. Saki, M. Toulany, W. Sihver, M. Zenker, J. M. Heldt, B. Mosch, H. J. Pietzsch, M. Baumann, J. Steinbach and H. P. Rodemann, *Strahlenther. Onkol.*, 2012, **188**, 823–832.
55 J. Harding and B. Burtness, *Drugs Today*, 2005, **41**, 107–127.
56 W. Sihver, J. Pietzsch, M. Krause, M. Baumann, J. Steinbach and H. J. Pietzsch, *Pharmaceuticals (Basel)*, 2014, **7**, 311–338.
57 S. R. Hubbard and W. T. Miller, *Curr. Opin. Cell Biol.*, 2007, **19**, 117–123.
58 J. Schlessinger, *Cell*, 2000, **103**, 211–225.
59 A. Gschwind, O. M. Fischer and A. Ullrich, *Nat. Rev. Cancer*, 2004, **4**, 361–370.
60 T. Holbro, G. Civenni and N. E. Hynes, *Exp. Cell Res.*, 2003, **284**, 99–110.
61 N. E. Hynes and G. MacDonald, *Curr. Opin. Cell Biol.*, 2009, **21**, 177–184.
62 G. Lurje and H. J. Lenz, *Oncology*, 2009, **77**, 400–410.
63 N. Tebbutt, M. W. Pedersen and T. G. Johns, *Nat. Rev. Cancer*, 2013, **13**, 663–673.
64 C. Yewale, D. Baradia, I. Vhora, S. Patil and A. Misra, *Biomaterials*, 2013, **34**, 8690–8707.
65 G. Gasser, in *Peptide Nucleic Acids: Methods and Protocols*, ed. P. E. Nielsen and D. H. Appella, Humana Press, 2014, vol. 1050, pp. 55–72.
66 G. Gasser, N. Hüsken, S. D. Köster and N. Metzler-Nolte, *Chem. Commun.*, 2008, 3675–3677.
67 T. Bruckdorfer, in *European Biopharmaceutical Review*, Spring, 2008, pp. 96, 98, 100, 102, 104.
68 K. P. García, K. Zarschler, L. Barbaro, J. A. Barreto, W. O'Malley, L. Spiccia, H. Stephan and B. Graham, *Small*, 2014, **10**, 2516–2529.
69 M. Hamidi, P. Rafiei and A. Azadi, *Expert Opin. Drug Discovery*, 2008, **3**, 1293–1307.

70 S. Jevsevar and R. Kontermann, Half-life extension through PEGylation Therapeutic Proteins, *Strategies to Modulate Their Plasma Half-life*, 2012.
71 K. Knop, R. Hoogenboom, D. Fischer and U. S. Schubert, *Angew. Chem., Int. Ed.*, 2010, **49**, 6288–6308.
72 F. Veronese and G. Pasut, *Drug Discovery Today*, 2005, **10**, 1451–1458.
73 J. M. Harris and R. B. Chess, *Nat. Rev. Drug Discovery*, 2003, **2**, 214–221.
74 P. Anstaett, Y. Zheng, T. Thai, A. M. Funston, U. Bach and G. Gasser, *Angew. Chem., Int. Ed.*, 2013, **52**, 4217–4220.
75 R. Bahal, N. A. McNeer, D. H. Ly, W. M. Saltzman and P. M. Glazer, *Artificial DNA: PNA & XNA*, 2013, **4**, 49–57.
76 G. M. Bonora, S. Drioli, M. Ballico, A. Faccini, R. Corradini, S. Cogoi and L. Xodo, *Nucleosides, Nucleotides Nucleic Acids*, 2007, **26**, 661–664.
77 A. Cattani-Scholz, D. Pedone, F. Blobner, G. Abstreiter, J. Schwartz, M. Tornow and L. Andruzzi, *Biomacromolecules*, 2009, **10**, 489–496.
78 M. Dettin, D. Silvestri, R. Danesin, E. Cretaio, G. Picariello, E. Casarin, A. Sonato, F. Romanato and M. Morpurgo, *Molecules*, 2012, **17**, 11026–11045.
79 J. M. Goldman, L. A. Zhang, A. Manna, B. A. Armitage, D. H. Ly and J. W. Schneider, *Biomacromolecules*, 2013, **14**, 2253–2261.
80 L. M. Kundu, H. Tsukada, Y. Matsuoka, N. Kanayama, T. Takarada and M. Maeda, *Anal. Chem.*, 2012, **84**, 5204–5209.
81 B. Sahu, I. Sacui, S. Rapireddy, K. J. Zanotti, R. Bahal, B. A. Armitage and D. H. Ly, *J. Org. Chem.*, 2011, **76**, 5614–5627.
82 Z. Zhang, Y. Liu, C. Jarreau, M. J. Welch and J.-S. A. Taylor, *Biomater. Sci.*, 2013, **1**, 1055–1064.
83 C. Foerster, M. Schubert, R. Bergmann, S. Vonhoff, S. Klussmann, M. Walther, J. Pietzsch, H.-J. Pietzsch and J. Steinbach, in *Technetium and Other Radiometals in Chemistry and Medicine*, ed. U. Mazzi, W. C. Eckelman and W. A. Volkert, SGEditoriali, Padova, Italy, 2010, pp. 357–362.
84 Y. Humblet, *Expert Opin. Pharmacother.*, 2004, **5**, 1621–1633.
85 B. Vincenzi, A. Zoccoli, F. Pantano, O. Venditti and S. Galluzzo, *Curr. Cancer Drug Targets*, 2010, **10**, 80–95.
86 T. M. Brand, M. Iida and D. L. Wheeler, *Cancer Biol. Ther.*, 2011, **11**, 777–792.
87 K. Zarschler, K. Prapainop, E. Mahon, L. Rocks, M. Bramini, P. M. Kelly, H. Stephan and K. A. Dawson, *Nanoscale*, 2014, **6**, 6046–6056.
88 C. S. Cutler, H. M. Hennkens, N. Sisay, S. Huclier-Markai and S. S. Jurisson, *Chem. Rev.*, 2013, **113**, 858–883.
89 E. W. Price and C. Orvig, *Chem. Soc. Rev.*, 2014, **43**, 260–290.
90 C. F. Ramogida and C. Orvig, *Chem. Commun.*, 2013, **49**, 4720–4739.
91 T. J. Wadas, E. H. Wong, G. R. Weisman and C. J. Anderson, *Chem. Rev.*, 2010, **110**, 2858–2902.
92 G. Liu, S. Zhang, J. He, N. Liu, S. Gupta, M. Rusckowski and D. J. Hnatowich, *Q. J. Nucl. Med.*, 2002, **46**, 233–243.
93 J. He, G. Liu, S. Dou, S. Gupta, M. Rusckowski and D. Hnatowich, *Bioconjugate Chem.*, 2007, **18**, 983–988.
94 W. H. Kuijpers, E. S. Bos, F. M. Kaspersen, G. H. Veeneman and C. A. van Boeckel, *Bioconjugate Chem.*, 1993, **4**, 94–102.
95 R. Alberto, R. Schibli, A. Egli, A. P. Schubiger, U. Abram and T. A. Kaden, *J. Am. Chem. Soc.*, 1998, **120**, 7987–7988.
96 J. Y. Song, S. W. Lee, J. P. Hong, S. E. Chang, H. Choe and J. Choi, *Cancer Lett.*, 2009, **283**, 135–142.
97 H. Björkelund, L. Gedda and K. Andersson, *PLoS One*, 2011, **6**, e16536.
98 Z. Novy, P. Barta, J. Mandikova, M. Laznicek and F. Trejtnar, *Nucl. Med. Biol.*, 2012, **39**, 893–896.
99 M. Azemar, M. Schmidt, F. Arlt, P. Kennel, B. Brandt, A. Papadimitriou, B. Groner and W. Wels, *Int. J. Cancer*, 2000, **86**, 269–275.
100 M. M. Moasser, A. Basso, S. D. Averbuch and N. Rosen, *Cancer Res.*, 2001, **61**, 7184–7188.
101 I. King and A. C. Sartorelli, *Cancer Res.*, 1989, **49**, 5677–5681.
102 D. T. Reardan, C. F. Meares, D. A. Goodwin, M. McTigue, G. S. David, M. R. Stone, J. P. Leung, R. M. Bartholomew and J. M. Frincke, *Nature*, 1985, **316**, 265–268.
103 K. Zarschler, S. Witecy, F. Kapplusch, C. Foerster and H. Stephan, *Microb. Cell Fact.*, 2013, **12**, 97.